

Review

# Asymmetric (Hot, Warm, Cold, Cryo) Rolling of Light Alloys: A Review

Denis Pustovoytov <sup>1</sup>, Alexander Pesin <sup>1,\*</sup> and Puneet Tandon <sup>2</sup>

<sup>1</sup> Laboratory of Mechanics of Gradient Nanomaterials, Nosov Magnitogorsk State Technical University, 455000 Magnitogorsk, Russia; pustovoytov\_den@mail.ru

<sup>2</sup> deLOGIC Lab, PDPM Indian Institute of Information Technology, Design and Manufacturing, Jabalpur 482005, India; ptandon@iiitdmj.ac.in

\* Correspondence: pesin@bk.ru; Tel.: +7-3519-063056

**Abstract:** Asymmetric sheet rolling is a process used when there are differences in any technological parameters in the horizontal plane across the width of the deformation zone or in the vertical plane between the top and bottom surfaces of the deformation zone. Asymmetry can either have random causes, or it can be created purposefully to reduce rolling force, improve sheet flatness, minimize the ski effect, obtain thinner sheets and for grain refinement and improvement of texture and mechanical properties of sheet metals and alloys. The purpose of this review is to analyze and summarize the most relevant information regarding the asymmetric (hot, warm, cold, cryo) rolling processes in terms of the effect of purposefully created asymmetry on grain size and mechanical properties of pure Mg, Al, Ti and their alloys. The classification and fundamentals of mechanics of the asymmetric rolling process are presented. Based on the analysis of publications related to asymmetric rolling, it was found that a superior balance of strength and ductility in pure Mg, Al, Ti and their alloys could be achieved due to this processing. It is shown that asymmetric rolling in comparison with conventional severe plastic deformation methods have an undeniable advantage in terms of the possibility of the production of large-scale sheets.



**Citation:** Pustovoytov, D.; Pesin, A.; Tandon, P. Asymmetric (Hot, Warm, Cold, Cryo) Rolling of Light Alloys: A Review. *Metals* **2021**, *11*, 956. <https://doi.org/10.3390/met11060956>

Academic Editor: Nikolay A. Belov

Received: 10 May 2021  
Accepted: 10 June 2021  
Published: 13 June 2021

**Publisher's Note:** MDPI stays neutral with regard to jurisdictional claims in published maps and institutional affiliations.

**Keywords:** asymmetric rolling; differential speed rolling; shear strain; severe plastic deformation; microstructure; mechanical behavior; Mg alloys; Al alloys; Ti alloys

## 1. Introduction

Asymmetric sheet rolling is a process used when there are differences in any technological parameters in the horizontal plane across the width of the deformation zone or in the vertical plane between the top and bottom surfaces of the deformation zone. Asymmetric rolling due to purposefully created differences in the circumferential speeds of the work rolls is also called “differential speed rolling”. For such a process, a degree of asymmetry is defined by a ratio of circumferential speeds  $V_1$  and  $V_2$  of the work rolls according to Equation (1):

$$S_R = \frac{V_1}{V_2} \quad (1)$$

where  $S_R$  is the “speed ratio” and  $V_1 > V_2$ . The first theoretical description of the asymmetric rolling process was proposed in 1941 by Siebel [1]. Experimentation has been used to quantify rolling force and torque. In 1947, Sachs and Klingler [2] first identified the region of cross shear, due to the fact that friction forces act in opposite directions in the deformation zone. The first invention of a rolling process with high ratio of circumferential speeds of work rolls ( $S_R = 3$ ) was announced in 1940 in the USSR by Razuvaev [3]. He was the first to propose a rolling process at a circumferential speed ratio equal to the ratio of sheet thicknesses before and after rolling according to Equation (2):

$$\frac{V_1}{V_2} = \frac{h_0}{h_1} \quad (2)$$



**Copyright:** © 2021 by the authors. Licensee MDPI, Basel, Switzerland. This article is an open access article distributed under the terms and conditions of the Creative Commons Attribution (CC BY) license (<https://creativecommons.org/licenses/by/4.0/>).

where  $h_0$  is the thickness of the sheet before the rolling pass,  $h_1$  is the thickness of the sheet after the rolling pass. This rolling process was proposed to reduce rolling force, obtain thinner sheets and reduce the number of rolling passes by increasing the reduction in each pass.

In the 1950s and 1960s, the first laboratory and industrial experiments on asymmetric rolling were performed and technological results were published [4,5]. Between the 1970s and 1990s, many experiments and theoretical calculations were carried out and the development of asymmetric rolling processes was focused mainly on the improvement of sheet geometry and technological aspects of the hot and cold rolling processes [6–13]. Asymmetry was used to reduce rolling force, improve sheet flatness, minimize the ski effect and obtain thinner sheets. Thus, from the 1940s to the end of the 1990s, the development of asymmetric rolling processes took place in research, which can be named as the “geometry approach” (Figure 1). The introduced asymmetry was rather low. Usually, the  $S_R$  value did not exceed 1.5. Since the end of the 1990s, a new direction in the research on the asymmetric rolling processes has occurred. The development of asymmetric rolling processes has taken place in research, which can be named as the “material approach”. The introduced asymmetry is rather high. Usually, the  $S_R$  value is more than or equal to 2.0.

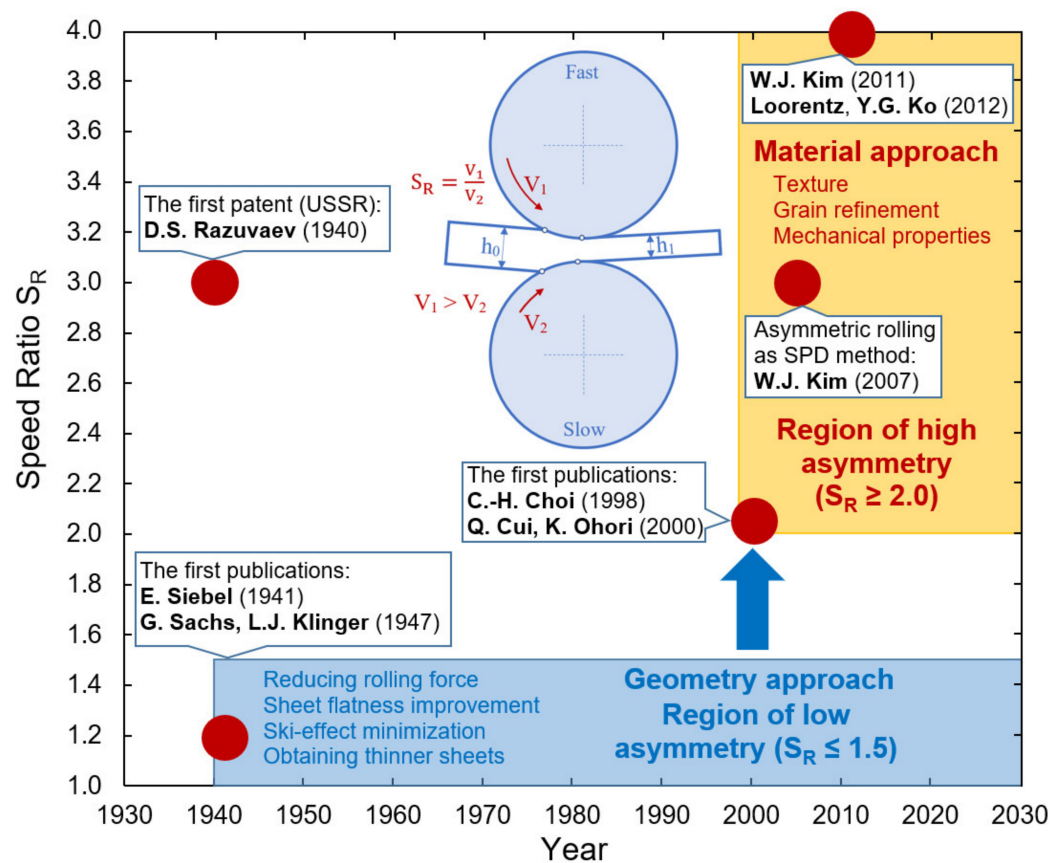


**Figure 1.** Different research lines for asymmetrical rolling processes: “geometry approach” and “material approach”.

The first work about using asymmetric rolling with a high speed ratio ( $S_R = 2.0$ ) to control the texture and mechanical properties of Al alloys was published in 1998 by Choi et al. [14]. It was shown that AA1100 and AA3005 sheets composed of only shear texture with high {111} components could be obtained by asymmetric rolling. A remarkable improvement in the average Lankford value was also obtained. In 2000, Cui and Ohori [15] demonstrated that the presence of shear strain is more important than the maximum level of thickness reduction, when considering grain refinement by asymmetric rolling. They

achieved grain refinement ( $\sim 2 \mu\text{m}$ ) in high-purity Al by asymmetric cold rolling. Fine grains evolved during asymmetric rolling and were stable at temperatures below 423 K.

In 2007, Kim et al. [16] introduced and developed an asymmetric rolling process known as the severe plastic deformation (SPD) method. Differential speed rolling with a high speed ratio ( $S_R = 3.0$ ) between the top and bottom work rolls was applied to AZ31 sheets (2 mm thick and 140 mm wide). The diameters of the top and bottom work rolls were identical and equal to 300 mm. From a starting thickness of 2 mm, sheets were reduced to 0.6 mm (70% reduction) by a single pass without lubrication. The effective strain accumulated during asymmetric rolling was 3.53 on average [16], which was comparable to that obtained by ECAP on a rod after three pressings. A very fine grain size of 1.4  $\mu\text{m}$  and a high yield stress of over 300 MPa were obtained after asymmetric rolling at 413 K. Significant grain refinement was achieved due to the introduction of high shear strain. The best compromise between strength and ductility was achieved at 433 K. This result indicated that SPD can be imposed by differential speed rolling with a high speed ratio. This process was called “high-ratio differential speed rolling” (HRDSR) [17–20]. In 2009, it was applied to obtain high-strength sheets from Al alloy 6061 [19], and in 2010, to obtain high-strength sheets from pure Ti [20]. Kim et al. [21] in 2011, Loorentz and Ko [22] in 2012 and Polkowski [23] in 2013 introduced differential speed rolling with speed ratio  $S_R = 4.0$  for improvement of the microstructure and texture in Ti [21], Al [22] and Cu [23] alloys.

Thus, from 1998 to the present, asymmetric rolling with the “material approach” has been applied to light alloys of Mg, Al and Ti, which are the materials selected for this review. These materials have very attractive features such as light weight and high specific strength. The development of asymmetric rolling technology, such as the severe plastic deformation method, for industrial production of large-scale sheets with ultrafine grain structure and enhanced mechanical properties has been the major research line for the last 20 years. Depending on temperature conditions, four asymmetric rolling processes can be implemented: (1) Asymmetric hot rolling, when the temperature of the sheet is in the range  $(0.6\text{--}0.8) T_{melt}$ , where  $T_{melt}$  is a melting temperature in K; (2) asymmetric warm rolling, when the temperature of the sheet is in the range  $(0.3\text{--}0.6) T_{melt}$ ; (3) asymmetric cold rolling, when the temperature of the sheet is below  $0.3 T_{melt}$ ; (4) asymmetric cryorolling, when the sheet is cooled in liquid nitrogen until the temperature reaches  $-153\text{--}-196 \text{ }^\circ\text{C}$ . Asymmetric cryorolling was first proposed in 2012 by Yu [24] as a new technique that combines the features of asymmetric rolling and cryorolling [25,26].

Although some reviews of asymmetric rolling processes have already been presented [27,28], the purpose of this review is to analyze and summarize the most relevant information regarding the asymmetric (hot, warm, cold, cryo) rolling processes in terms of the effect of purposefully created asymmetry on grain size and mechanical properties of pure Mg, Al, Ti and their alloys. This work is divided into six sections. First, the classification of asymmetric rolling processes is presented. Secondly, the fundamentals of the mechanics of the asymmetric rolling process due to purposefully created differences in the peripheral speeds of the work rolls are presented. This is followed by an analysis of asymmetric (hot, warm, cold, cryo) rolling of Mg alloys, Al alloys and Ti alloys. The review ends with conclusions and future prospects for these technologies.

## 2. Classification of Asymmetric Rolling Processes

Asymmetry can either have random causes, or it can be created purposefully (Figure 2). Asymmetry in the horizontal plane along the width of the deformation zone due to random causes can be caused by differences in thickness, temperatures, friction, displacement of the sheet along the work roll length, skewed work rolls or incorrect setting of the right and left hydraulic pressure devices.

Asymmetry in the vertical plane between the top and bottom surfaces of the deformation zone due to random causes can be caused by inclined entry of the sheet into the roll gap, differences in temperatures, friction, differences in the work roll diameters at the same angular speeds or differences in the work roll angular speeds with the same diameters. In

any case, asymmetric rolling caused by random causes is undesirable. For example, a negative consequence of asymmetric rolling is the bending of the plate, usually in hot rolling mills, more often known as the “ski effect” [29,30]. The negative effect of such asymmetry is prevented by improving equipment, stabilizing technology and using automatic regulators. However, asymmetry can also be purposefully introduced to improve the rolling process, for example, reducing rolling force, improving sheet flatness, minimizing the ski effect, obtaining thinner sheets, grain refinement and improvement of the texture and mechanical properties of sheet metals and alloys.

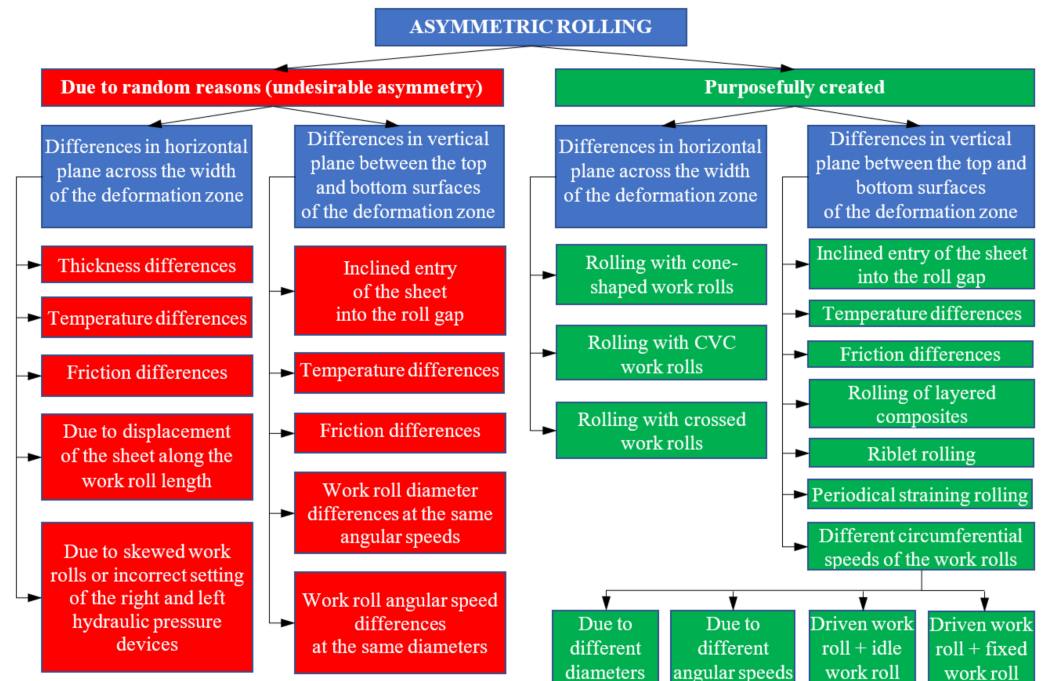


**Figure 2.** Classification of asymmetric rolling processes.

Asymmetry in the horizontal plane across the width of the deformation zone can be purposefully created by rolling with cone-shaped work rolls [31]. A schematic illustration of this process is shown in Figure 3a. When the ratio of the largest diameter of the roll to the smallest one  $D/d = 1.5$ , shear strain increases by 1.5–2.0 times in comparison with conventional rolling [32].

A little asymmetry in the horizontal plane across the width of the deformation zone can be an effective tool to improve sheet shape. The continuous variable crown (CVC) system (Figure 3b) was developed by Schloemann-Siemag (SMS) as a powerful tool for sheet shape control. The work rolls have an “S” shape and are arranged asymmetrically [33]. Through the axial shifting of two work rolls towards each other, a continuously adjustable rolling gap contour can be obtained. The CVC system is employed in many cold rolling and hot rolling mills worldwide. A little asymmetry in the horizontal plane can also be obtained by crossed work rolls (Figure 3c). The first hot rolling mill with asymmetry due to crossed work rolls was used at Nippon Steel’s Kimitsu Works in 1991 [34]. In the work roll crossed system, the axes of the top and bottom work rolls are crossed as shown in Figure 3c. Work roll crossing is designed to control the roll gap profile. This action provides control over the shape and profile of the sheet. Thus, a little asymmetry across the width of the deformation zone provided by CVC or crossed work rolls is used in industrial rolling mills to improve the shape and flatness of sheets.

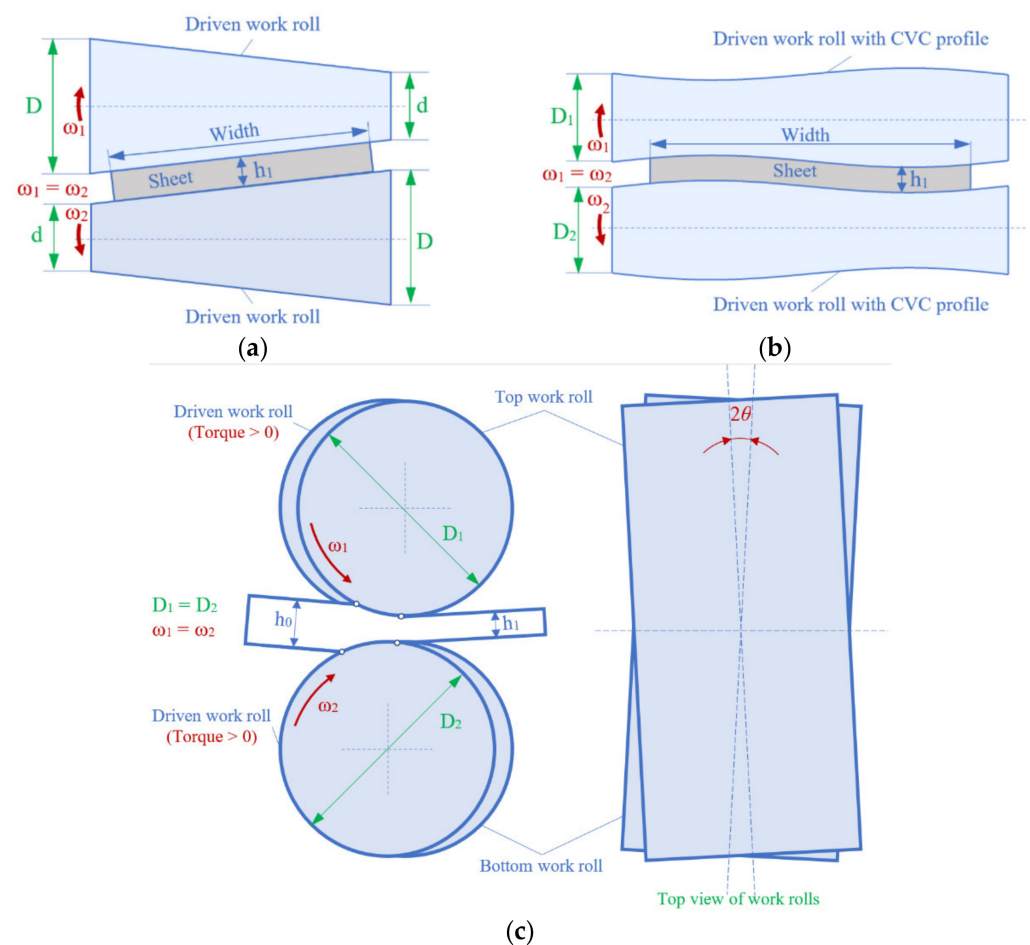


**Figure 3.** Schematic illustration of asymmetric rolling processes with purposefully created asymmetry in the horizontal plane along the width of the deformation zone: (a) Rolling with cone-shaped work rolls; (b) rolling with CVC work rolls; (c) rolling with crossed work rolls.

Asymmetry in the vertical plane between the top and bottom surfaces of the deformation zone can be purposefully created by inclined entry of the sheet into the roll gap [35] (Figure 4a) or due to differences in temperatures, when one work roll is purposefully heated and the other one is cold (Figure 4b).

Asymmetry during rolling can be purposefully created due to friction differences [36,37]. This rolling process is called “differential friction rolling” [37]. To change the friction coefficients on the contact surfaces of the deformation zone, the lubricant can be supplied only from one side (Figure 5a). Another way to create friction differences is rolling with different roughnesses of the top and bottom work rolls (Figure 5b). Utsunomiya et al. [37] proposed a differential friction rolling process for improvement in the  $r$ -value of aluminum sheets. A two-high rolling mill with TiC-coated rolls 130 mm in diameter was used for rolling of commercial aluminum AA1050 sheets 3 mm thick and 30 mm wide. A single-pass thickness reduction of 50% was conducted at 473 K. Low friction was achieved by applying a thin polytetrafluoroethylene (PTFE) film on the sheet. Teflon (PTFE) was sprayed by aerosol on the upper surface of the aluminum sheet and dried. However, the lower surface remained unlubricated. Both the top and bottom rolls revolved at the same speed of 2 m/min. The shear strain introduced by differential friction rolling was comparable to that introduced by differential speed rolling [37]. The annealed sheet showed a higher  $r$ -value than the symmetrically rolled sheet.

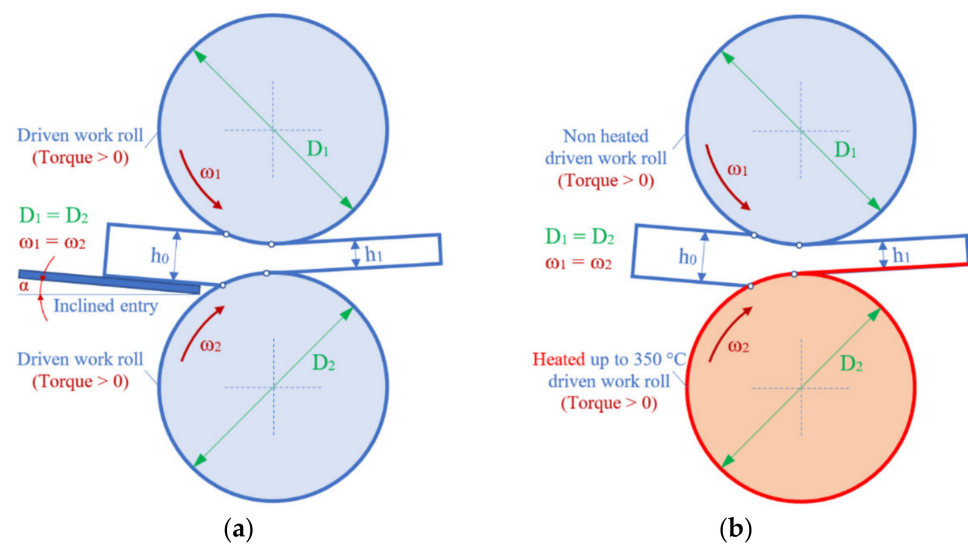


**Figure 4.** Schematic illustration of asymmetric rolling processes: (a) Rolling with inclined entry of the sheet into the roll gap; (b) rolling with temperature differences.

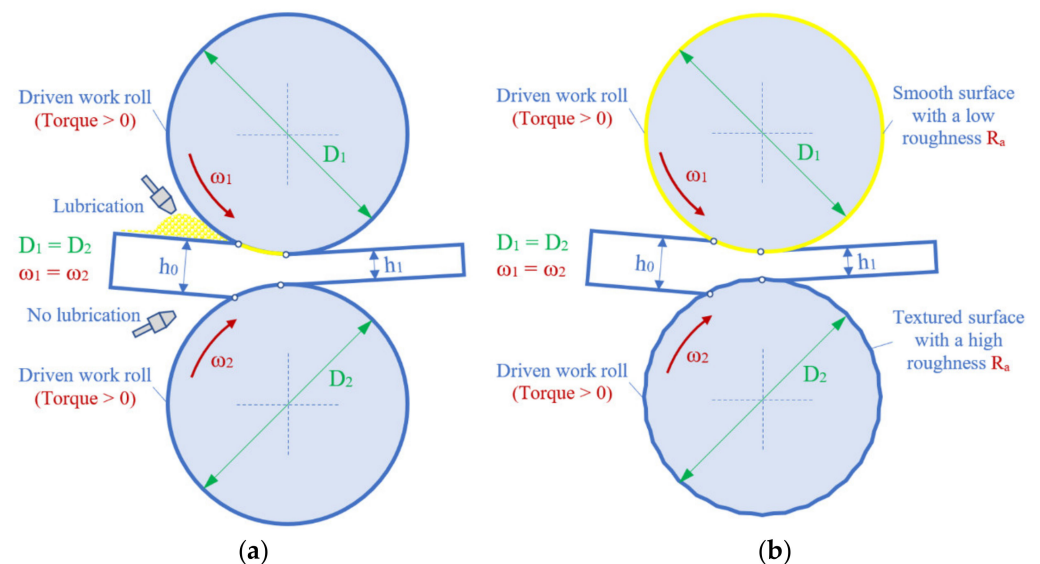


**Figure 5.** Schematic illustration of asymmetric rolling processes due to friction differences: (a) Rolling with different lubrications for top and bottom work rolls; (b) rolling with different roughnesses of top and bottom work rolls.

Asymmetry during rolling can be purposefully created due to differences in the circumferential speeds of the work rolls. Asymmetric rolling can be implemented due to disconnecting one work roll to make another work roll the only driven work roll (Figure 6a). This process called “single-roll-driven rolling” [38]. Sakai et al. [39] proposed two-pass single-roll-driven unidirectional shear rolling. Shear strain greater than 1.0 was introduced throughout the thickness of the AA5052 sheet. A shear texture was developed throughout the thickness of the sheets. The average  $r$ -value equaled unity. These values resulted in a superior drawability of the unidirectionally shear rolled and annealed sheets to that of sheets fabricated by the conventional process.

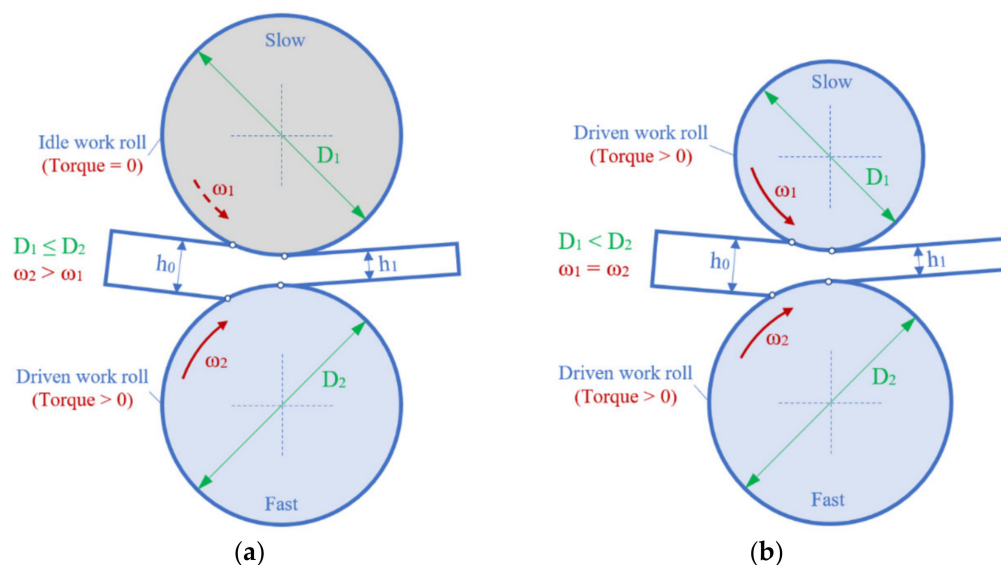


**Figure 6.** Schematic illustration of asymmetric rolling processes due to different circumferential speeds of the work rolls: (a) Rolling with idle work roll (“Single roll driven rolling”); (b) rolling with different diameters of top and bottom work rolls.

Asymmetry can also be achieved by using work rolls with different diameters while rotating at the same angular speed (Figure 6a). Choi et al. [14] used asymmetric rolling with different diameters of 248 mm and 126 mm of the top and bottom work rolls to control the texture and mechanical properties of Al alloys. Pesin [40] developed an improved process of asymmetric rolling by using different diameters of work rolls in combination with a bending roll (Figure 7a). This process is called the “combined process of asymmetric rolling and plastic bending”. This technology is used to produce segments of large cylinders (Figure 7b) as curved plates with an angular size of 45 . . . 60 degrees, plate thickness of 40 . . . 220 mm, a width of up to 4300 mm, a length of up to 5000 mm and a radius of curvature from 1850 to 5000 mm. Industry testing of the combined process of asymmetric rolling and plastic bending is shown in Figure 8.

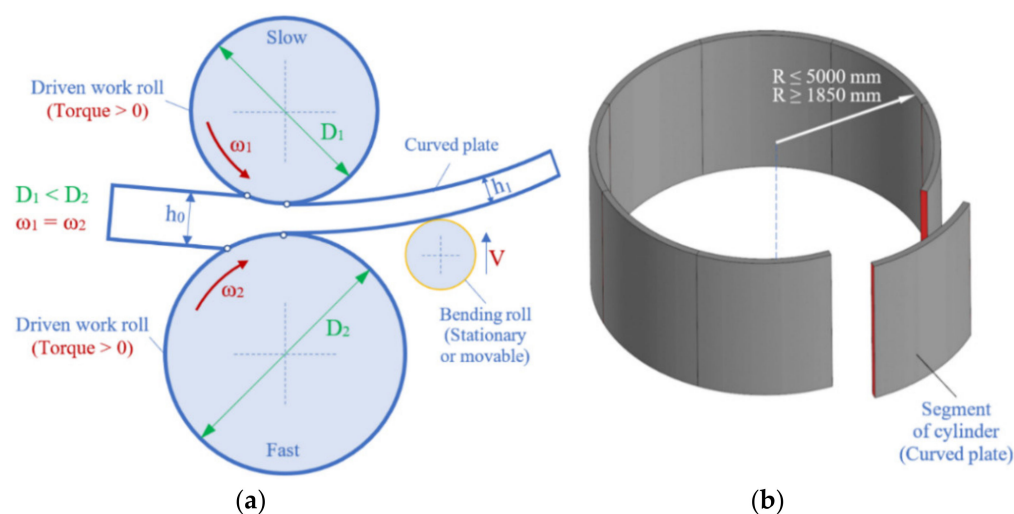


**Figure 7.** Schematic illustration of combined process of asymmetric rolling and plastic bending (a) and a curved plate as a segment of a cylinder (b).

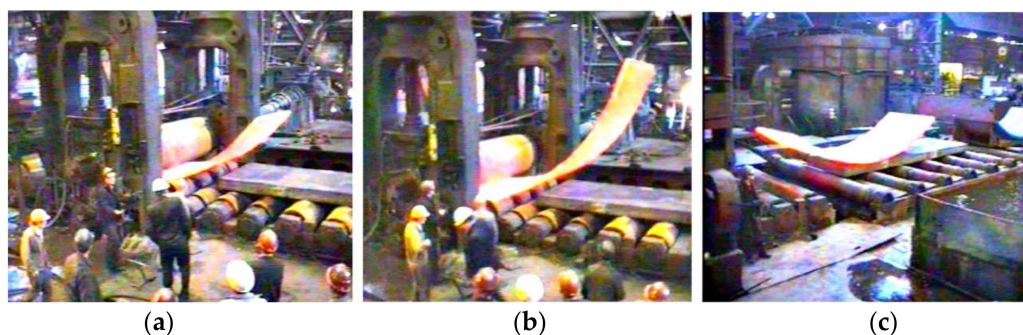


**Figure 8.** Industry testing on hot plate mill 4500 at OJSC Magnitogorsk Iron and Steel Works: (a,b) Combined process of asymmetric rolling and plastic bending; (c) finished curved plate.

Asymmetric rolling can be achieved by using a single driven work roll, when one of the rolls is kept stationary. In the late 1970s, Potapkin and Fedorinov [41] proposed an asymmetric rolling process called “deformation by a stationary and driven work roll” (Figure 9a). The process is carried out at a sufficiently high front tension of the strip. The diameter of the stationary work roll is 3–10 times smaller than the diameter of the driven work roll. This provides a significant reduction in rolling force due to a decrease in the contact area. The technological capabilities and advantages of this process increase with a decrease in the diameter of the stationary roll. However, this decrease is limited by a decrease in its strength and rigidity and complications of fastening (the possibility of work roll twisting). In the late 1980s, Pesin [42] proposed to use, instead of a stationary cylindrical work roll, a prism-shaped tool with a cylindrical part with a very small radius up to 5 mm (Figure 9b). This solves the problem of the strength and rigidity of the deforming tool in combination with ensuring a small radius of the contact surface of this tool.

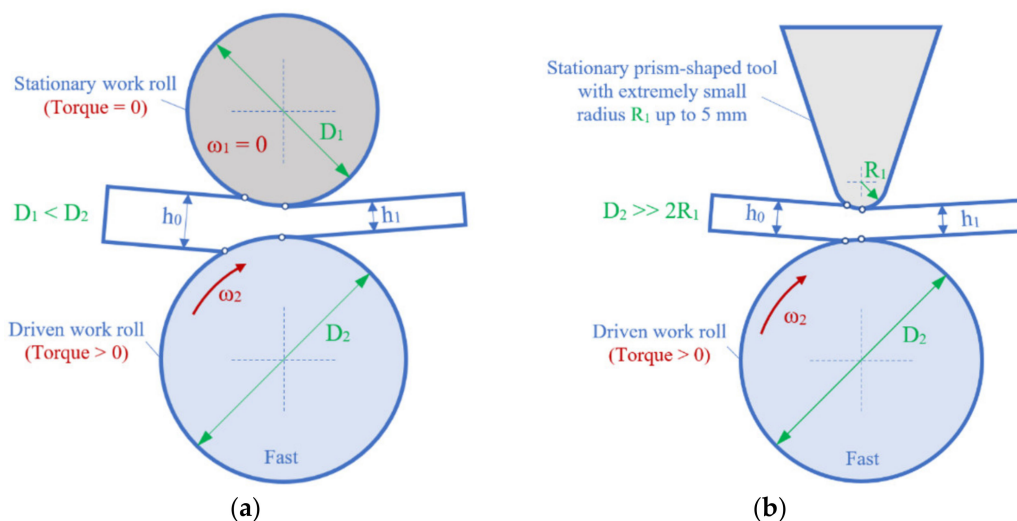


**Figure 9.** Schematic illustration of asymmetric rolling processes: (a) Deformation by a stationary and driven work roll; (b) deformation by a stationary prism-shaped tool and driven work roll.

Asymmetric rolling can be carried out due to different angular speeds of the work rolls with the same diameters (both rolls are driven) (Figure 10a). The ratio of these speeds is one of the most important parameters of the process, since it will influence the velocity field along the sheet thickness (together with other parameters, such as contact friction and thickness reduction per pass). The asymmetric rolling due to purposefully created differences in the circumferential speeds of the work rolls is also called “differential speed rolling”.

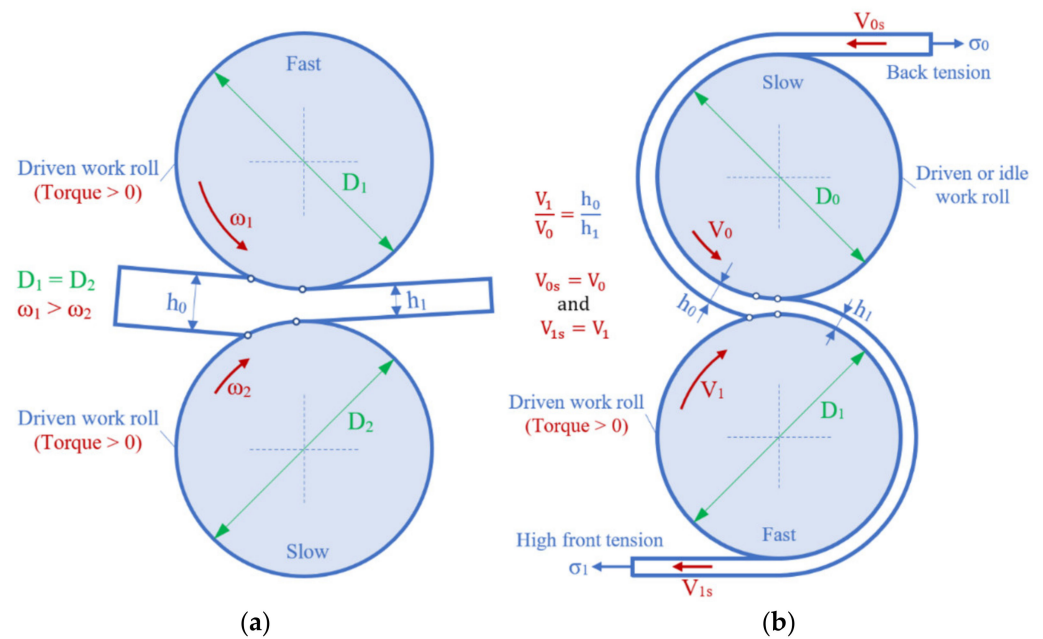


**Figure 10.** Schematic illustration of asymmetric rolling processes due to different circumferential speeds of the work rolls: (a) Rolling with different angular speeds of the work rolls; (b) “rolling–drawing” process.

In the 1960s and 1970s, the energy theory of the asymmetric rolling process was developed by Vydrin [43]. As a result, a new asymmetric rolling process called “rolling–drawing” (Figure 10b) was proposed in 1971 [44]. This process is carried out under the following kinematic conditions:

$$\frac{V_1}{V_0} = \frac{h_0}{h_1}, V_{0s} = V_0 \text{ and } V_{1s} = V_1 \quad (3)$$

where  $V_{0s}$ ,  $V_{1s}$  are the circumferential speeds of the strip before and after the deformation zone, respectively;  $V_0$ ,  $V_1$  are the circumferential speeds of the work rolls;  $h_0$  is the thickness of the strip before the rolling pass;  $h_1$  is the thickness of the strip after the rolling pass. The rolling–drawing process is carried out at a sufficiently high front tension of the strip. Such kinematic conditions provide one-zone and counter-directional friction forces in the deformation zone. Since the rolling–drawing process requires a high front tension of the strip, the thickness reduction per pass should not exceed 10–40%. This limits the possibility of using this process.

Thus, different circumferential speeds of the work rolls can be created in the following ways: (1) due to different diameters of the work rolls at the same angular speeds (both rolls are driven); (2) when one work roll is driven and another work roll is idle; (3) when one work roll is driven and another work roll or tool is stationary; (4) due to different angular speeds of the work rolls with the same diameters (both rolls are driven). The main disadvantage of the first three ways is the low technological flexibility of these processes due to the impossibility to control the speed ratio  $S_R$  of the work rolls when creating shear strain, which is necessary for grain refinement and improving the texture and mechanical properties of various metals and alloys. From an industrial point of view, rolling with different angular speeds of the work rolls with the same diameters (both rolls are driven) is the most suitable way to implement asymmetric rolling.

Asymmetry during rolling can be purposefully created due to differences in the surface geometry of the top and bottom work rolls. In 2014, Shimoyama et al. [45] proposed the new rolling process called “periodical straining rolling” that enables control of the microstructure and texture of Mg alloys sheets. The periodical straining rolling process consists of two deformation stages. At the first pass, the sheet is rolled with a grooved

work roll with, for example, a sine profile of the surface, and a flat work roll (Figure 11a). As a result, small rack-like dimples are formed periodically on the sheet surface. At a subsequent rolling pass, the rack-like sheet is flattened by conventional flat work rolls. Finally, the smooth sheet surface is obtained. The objective of the proposed rolling process is to introduce localized strain, to cause microstructure and texture changes in the rolled sheet. Periodical straining rolling can be easily adapted in existing strip rolling mills by replacing the ordinary work roll profiles.

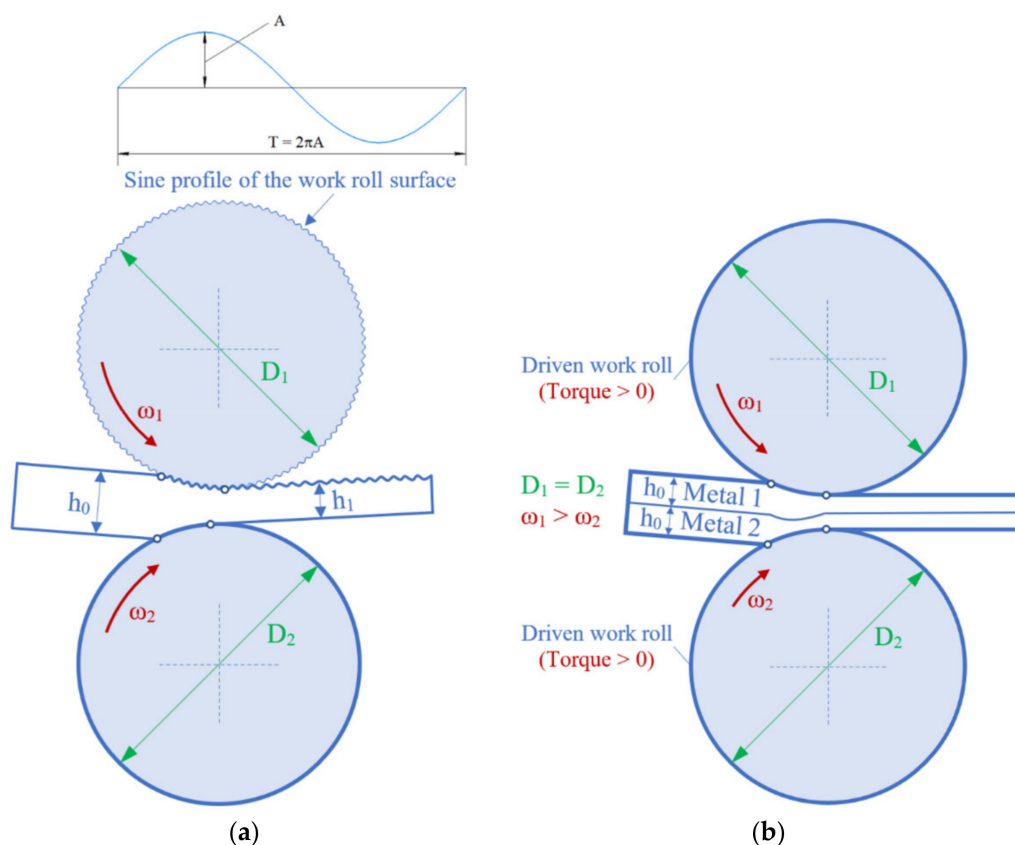


**Figure 11.** Schematic illustration of periodical straining rolling (a) and asymmetric roll bonding of bimetal layered composites (b).

Hot or cold rolling is widely used for the manufacturing of bimetal layered composites [46]. As a result of the difference between the flow stresses of the sheets to be bonded, this process belongs essentially to the category of asymmetric rolling. However, this process is usually simply called “hot or cold roll bonding”. Additional purposefully created asymmetry due to different circumferential speeds of the work rolls can be introduced to the rolling process of bimetal layered composites [47]. In this case, the rolling process is called “asymmetric hot or cold roll bonding” (Figure 11b). The harder metal contacts the fast work roll and the softer metal contacts the slow work roll. The deformation zone of asymmetric rolling forms a cross shear zone, which increases the bonding strength.

In 2019, Wang [48–50] proposed the new asymmetric rolling process called “corrugated rolling and flat rolling” (Figure 12) to achieve strong interface bonding and substantial grain refinement in Mg/Al and Cu/Al layered composites. The surface of a corrugated work roll was designed as a sine curve with an amplitude of 0.5 mm and a period of 0.06 radians. The diameters of the corrugated and flat work rolls were both 150 mm [48].

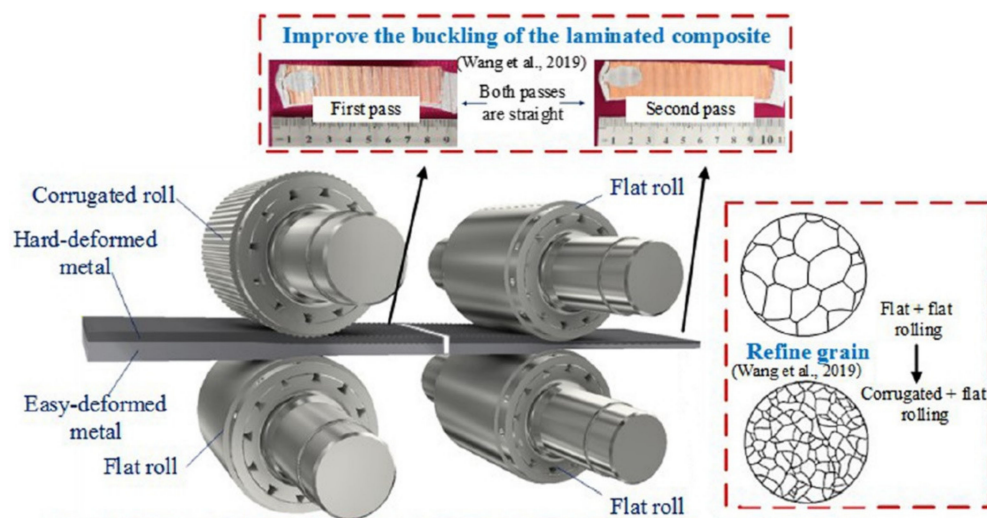


**Figure 12.** Schematic illustration of corrugated rolling and flat rolling, reproduced from [50], with permission from Elsevier, 2021.

During the first corrugated rolling, compressive stress of various orientations is formed in the corrugated Mg/Al laminated composite [49]. This means that asymmetric deformation occurs, as shown in Figure 13 [49]. The upper corrugated roll results in an inhomogeneous local stress distribution at different positions. Thus, the grain structure of AZ31B might not be uniform and the microstructure might change with the curve of the corrugated roll. On the contrary, the lower conventional flat roll corresponds to 5052 aluminum and stresses on the aluminum sheet near the flat roll appear to be homogeneous. During the second flattened rolling process, the AZ31B metal at the peak position prepared by the first pass flows downward and sideways, enduring severe plastic deformation under the rolling force. The original coarse grain might be broken and recrystallize during the rolling process and subsequent heat treatment. Considering the matching of surface ripples between the corrugated Mg/Al composite and corrugated roll, the rolling force appears to be uniform along the width direction, which is different from the force along the rolling direction. Therefore, for the flattened as-rolled Mg/Al laminated composite, the longitudinal and transverse interfacial microstructures are significantly different. The Mg/Al laminated composites prepared by corrugated rolling and flat rolling exhibited outstanding tensile properties along both RD and TD, which can be attributed to the microstructure refinement induced by the severe shear strain. The tensile properties along TD were higher than that along RD in both the as-rolled and heat-treated state, and this significant anisotropy of the tensile property was mainly due to the microstructure spatial distribution and the interfacial intermetallic compound layer along the different directions [49].

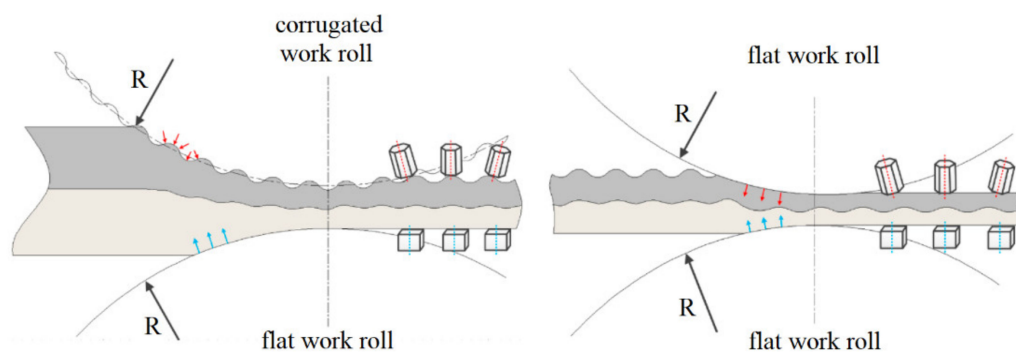


**Figure 13.** Schematic illustration showing the shear stress during the corrugated rolling and flat rolling process [49].

Pesin et al. [51] proposed asymmetric rolling based on the corrugated rolling and flat rolling process for the manufacturing of Al–steel layered composites with improved bonding strength between the stacked layers. It was numerically shown [51] that mechanical clinching and elevated plastic strain at the interface due to the creation of wave-like contact surfaces between the Al and steel, with the mutual penetration of hard material into soft material when the shear strain is activated, can provide superior bonding strength.

In 2007, Hirt and Thome [52,53] proposed the new asymmetric rolling process called “riblet rolling”, which is used to obtain specific functional surface structures. Before rolling, a fine high-strength steel wire is tightly wound around the upper roll to provide it with a negative riblet imprint. Afterwards, the riblet structure is formed on the sheet by riblet rolling (Figure 14). The aim is to approach the production of semi-circular shaped riblet structures with a spacing  $s$  of 90–100  $\mu\text{m}$ . In the ideal case, the ratio of riblet height  $h$  to riblet spacing  $s$  should be about 0.5. Riblet spacing  $s$  is defined by the diameter  $d_w$  of the used steel wire. This surface is characterized by almost perfect negative semi-circular riblet structures with very sharp ground radii. The accuracy of the winding process—i.e., a constant pitch  $p$  of the steel wire on the roll—must be very high.

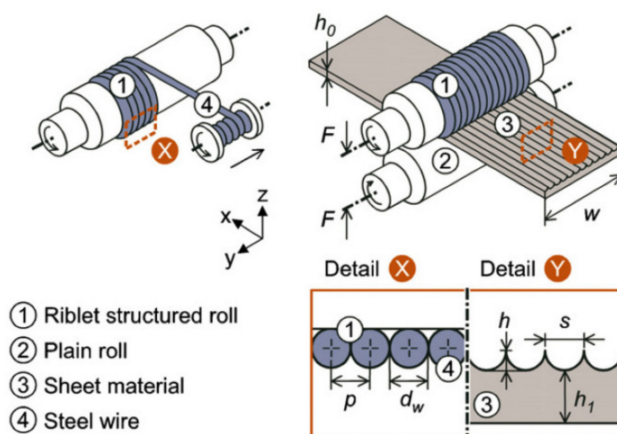


**Figure 14.** Schematic illustration of riblet rolling, reproduced from [52], with permission from Elsevier, 2008.

Rolling of functional riblet structures allowing for significant drag reduction on surfaces in fluid dynamic applications like airplanes and trains can be applied for the manufacturing of aluminum alloy sheets. Polished cross-sections of structured clad and bare AA 2024-T351 sheets are shown in Figure 15 [54]. Rolling of uniformly shaped riblets with a lateral distance of less than 100  $\mu\text{m}$  is assumed to be possible on large Al sheets.

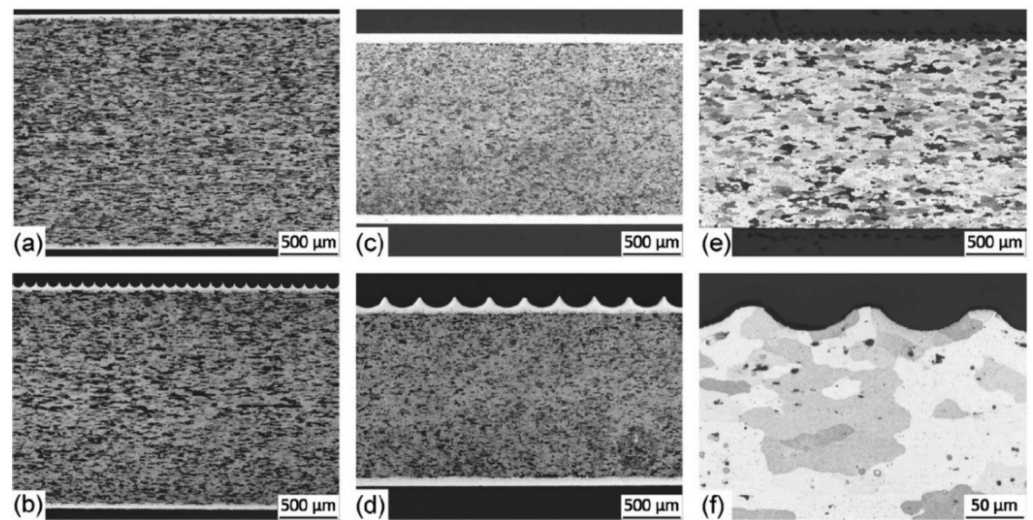


**Figure 15.** Polished cross-sections. (a) A 2 mm thick AA 2024-T351 sheet combined with a clad layer of commercially pure Al (Alclad 2024-T351). (b) Structured sheet of Alclad 2024-T351 with 80  $\mu\text{m}$  riblet diameter. (c) A 1.6 mm thick Alclad 2024-T351 sheet. (d) Structured sheet of Alclad 2024-T351 with 300  $\mu\text{m}$  riblet diameter. (e,f) A 2 mm thick AA2024-T351/T4 bare sheet with 100  $\mu\text{m}$  riblet diameter, reproduced from [54], with permission from Elsevier, 2014.

### 3. Fundamentals of Differential Speed Rolling

#### 3.1. Deformation Zone

The sheet is deformed in the deformation zone between the entrance and the exit, where the initial thickness  $h_0$  is reduced to the final thickness  $h_1$ , as shown in Figure 16. During symmetric rolling, as shown in Figure 16a, the circumferential speed of the bottom work roll  $V_1$  equals a circumferential speed of the top work roll  $V_2$ , and the speed of the bottom surface of the sheet  $V_{1s}$  equals the speed of the top surface of the sheet  $V_{2s}$ . The neutral points on the top and bottom contact surfaces are at the same locations in the direction of rolling. Neutral points divide the deformation zone into two zones: a backward slip zone and a forward slip zone. In the backward slip zone, the contact friction forces are active, and in the forward slip zone, they are reactive. If pressure  $p$  or the shear strength  $k$  is known at the contact surface, the frictional stress  $\tau$  can be expressed as  $\mu p$  in accordance with the Coulomb friction law or  $mk$  in accordance with the shear friction law. Here,  $\mu$  is the Coulomb friction coefficient and  $m$  is the shear friction factor. During differential speed rolling when  $V_1$  is greater than  $V_2$ , the neutral point associated with the slow work roll is shifted toward the entrance of the roll gap, while the neutral point associated with the fast work roll is moved toward the exit of the roll gap (Figure 16b). As a result, along with the backward slip zone and the forward slip zone, a third zone appears—the cross-shear zone—in which the forces of contact friction are oppositely directed.

Depending on length of the backward and forward slip zones from the side of the top and bottom work rolls, the following cases of differential speed rolling may occur:

- (1) General case, when the deformation zone is divided into three zones: backward slip zone, forward slip zone and cross-shear zone (Figure 16b). There are two neutral points in the deformation zone.
- (2) Semi-limiting case, when the deformation zone is divided into two zones: backward slip zone or forward slip zone and cross-shear zone. In this case, one neutral point is between the entrance and exit of the deformation zone, and the other neutral point is at the entrance or at the exit of the deformation zone. This neutral point may also be completely absent. This case corresponds to the asymmetric rolling due to deformation by a stationary and driven work roll (Figure 9a) or due to deformation by a stationary prism-shaped tool and driven work roll (Figure 9b).

- (3) Limiting case, when only the cross-shear zone occupies the entire deformation zone. The first neutral point is at the entrance of the deformation zone, and the second neutral point is at the exit of the deformation zone. This case corresponds to the rolling–drawing process which requires a high front tension, as mentioned above (Figure 10b).

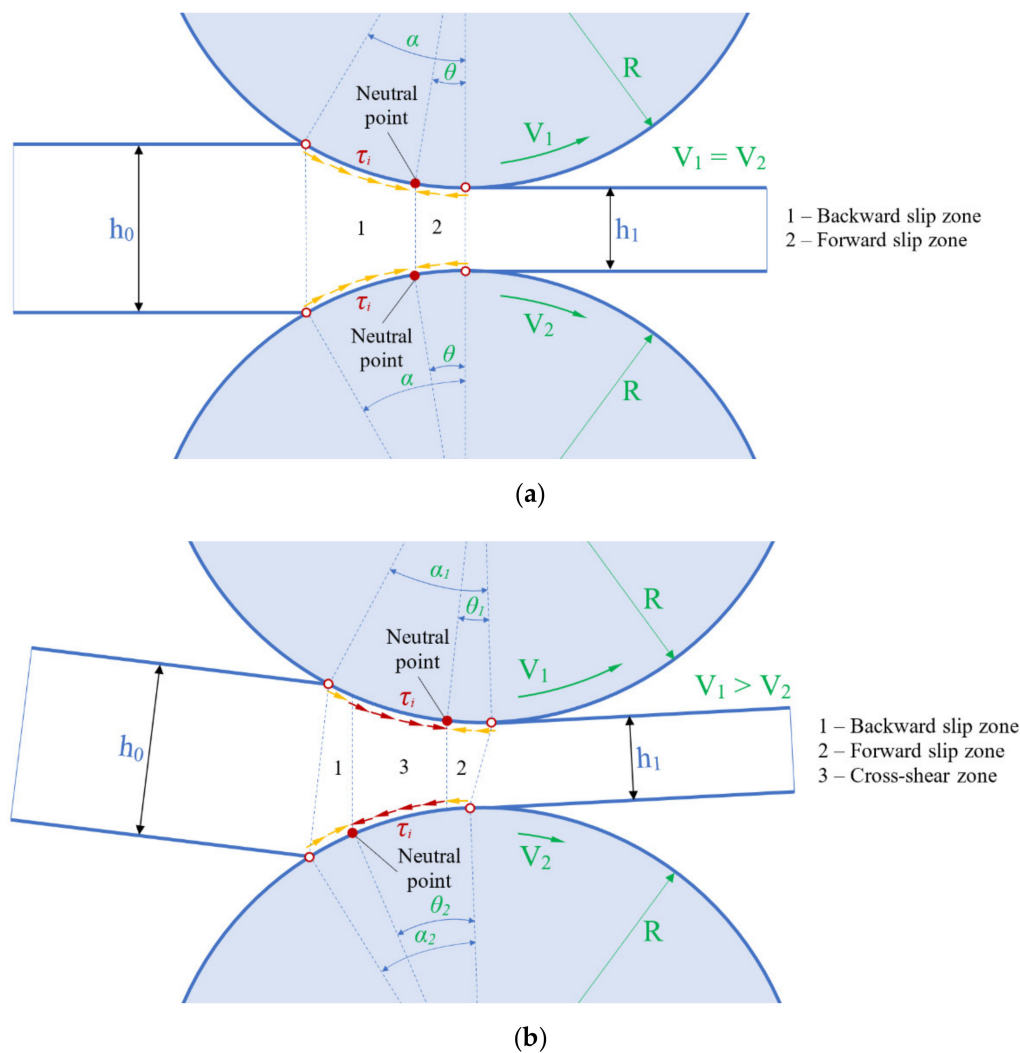


**Figure 16.** Schematic illustration of deformation zone during symmetric (a) and differential speed rolling (b).

In symmetric rolling, the pressure distribution at the work roll/sheet interface has a typical “friction hill”. The rolling pressure increases gradually from the entrance of the deformation zone, reaches a maximum value corresponding to the neutral point and then gradually falls towards the exit of the deformation zone. In asymmetric rolling, the “friction hill” is cut off due to the cross-shear zone. As a result, rolling force is decreased. This is one of the main advantages of asymmetric rolling. Figure 17 shows pressure distribution along the deformation zone during symmetric and asymmetric rolling. Zuo et al. [55] reported that in the case of hot asymmetric rolling of aluminum alloy 5182, the rolling force was 5–30% lower than that of symmetric hot rolling. It was also confirmed by Tian et al. [56] that the extent of the cross-shear zone increases with the increase in the circumferential speed ratio, whereas the rolling force decreases.

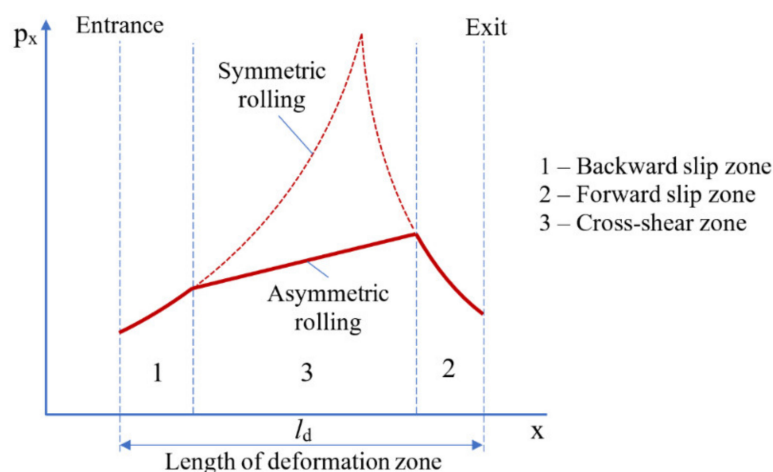


**Figure 17.** Schematic illustration of pressure distribution along the deformation zone during symmetric and asymmetric rolling.

### 3.2. Dissipation of Power and Speed Profiles in Deformation Zone

The power provided by the faster work roll is represented in Figure 18 by the area of a-e-e'-d-a minus the area of e-b''-c-e'-e multiplied by the frictional stress, while that by the slower work roll is the area of a''-f-f'-d-a'' minus the area of f-b'-c-f'-f multiplied by the frictional stress [57]. The power used for deformation by the faster work roll is the area of a'-g-e-e'-d-a' minus the area of e-b-c-e'-e multiplied by the frictional stress, while that by the slower work roll is the area of a'-f-f'-d-a' minus the area of f-g'-b-c-f'-f multiplied by the frictional stress. The power wasted by friction is the power provided by work rolls minus the power used for deformation. In particular, the power used for shear deformation due to the differential speed is represented by the area of a'-g-b-g'-a' multiplied by the frictional stress [57].

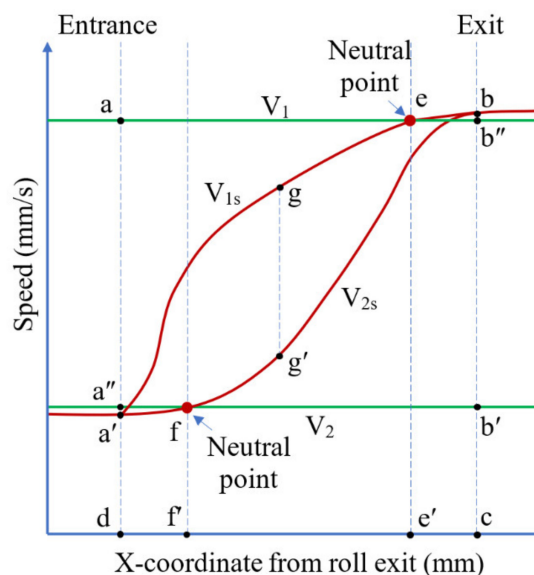


**Figure 18.** Schematic illustration of speed profiles in deformation zone during differential speed rolling, reproduced from [57], with permission from Elsevier, 2015.

Park [57] suggests Relation (4) that restricts the speed ratio to be less than the thickness ratio. If this relation is not satisfied, a portion of the power provided by the rolls becomes unnecessarily wasted as frictional heat, rather than used for deformation of the sheet.

Additionally, an excessive tensile stress could be developed in the sheet, resulting in fracture if the material of the sheet is as brittle as a magnesium alloy.

$$\frac{V_1}{V_0} < \frac{h_0}{h_1} \tag{4}$$

where  $V_0, V_1$  are the circumferential speeds of the work rolls;  $h_0, h_1$  are the thickness of the sheet before and after rolling.

### 3.3. Shear Strain and Equivalent Strain

The level of a shear strain and equivalent strain plays a key role in terms of the possibility of using the asymmetric rolling process as a method of SPD. Two types of shear strain are known: pure shear and simple shear. Pure shear corresponds to symmetric rolling. During pure shear, the square is converted to a rectangle and the circle is converted to an ellipse (Figure 19). The thickness “AB” is compressed, and the length “AD” is elongated. The axes of the strain ellipsoid do not rotate (Figure 20).

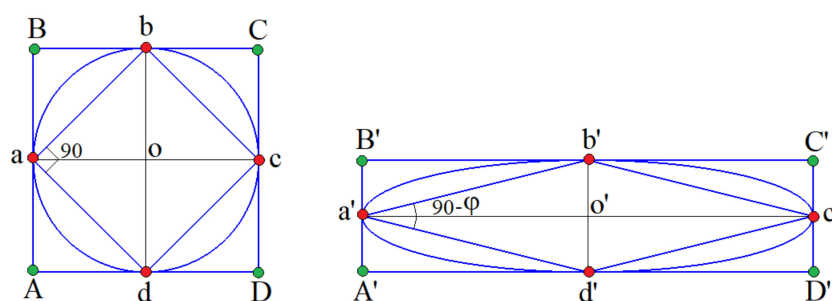


Figure 19. Schematic illustration of pure shear during symmetric rolling.

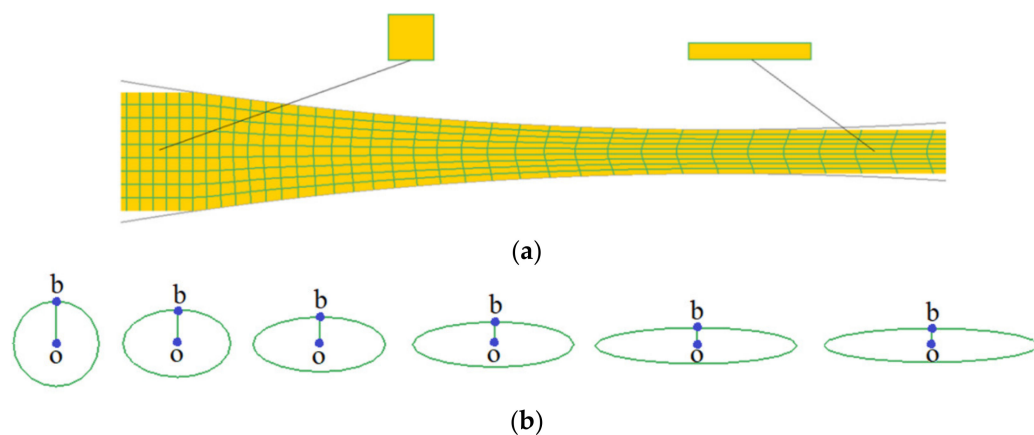


Figure 20. FEM simulation (this work) of pure shear during symmetric rolling (a) and transformation of strain ellipsoid (in the middle layer) when passing through the deformation zone (b).

Simple shear corresponds to equal channel angular pressing (ECAP) (Figure 21). During simple shear, the square is converted to a parallelogram and the circle is converted to an ellipse (Figure 22). The thickness “AB” and the length “AD” are not changed. Simple shear involves rotation of the axes of the strain ellipsoid (Figure 23). Exact rotation leads to grain refinement and the formation of high angle boundaries during ECAP.

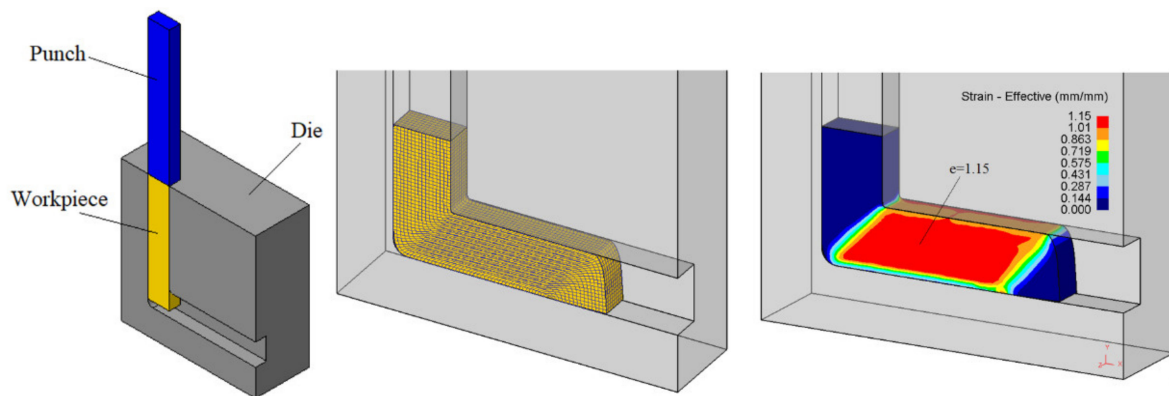


Figure 21. Schematic illustration of ECAP.

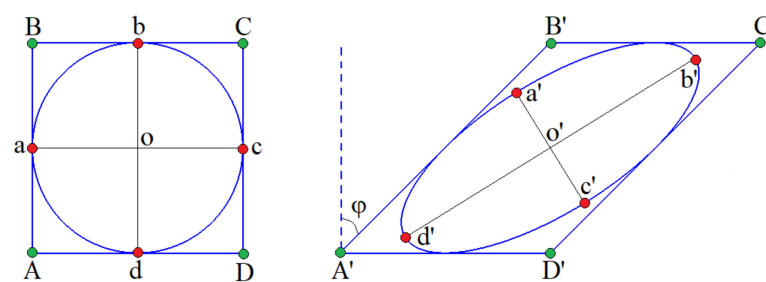


Figure 22. Schematic illustration of simple shear during ECAP.

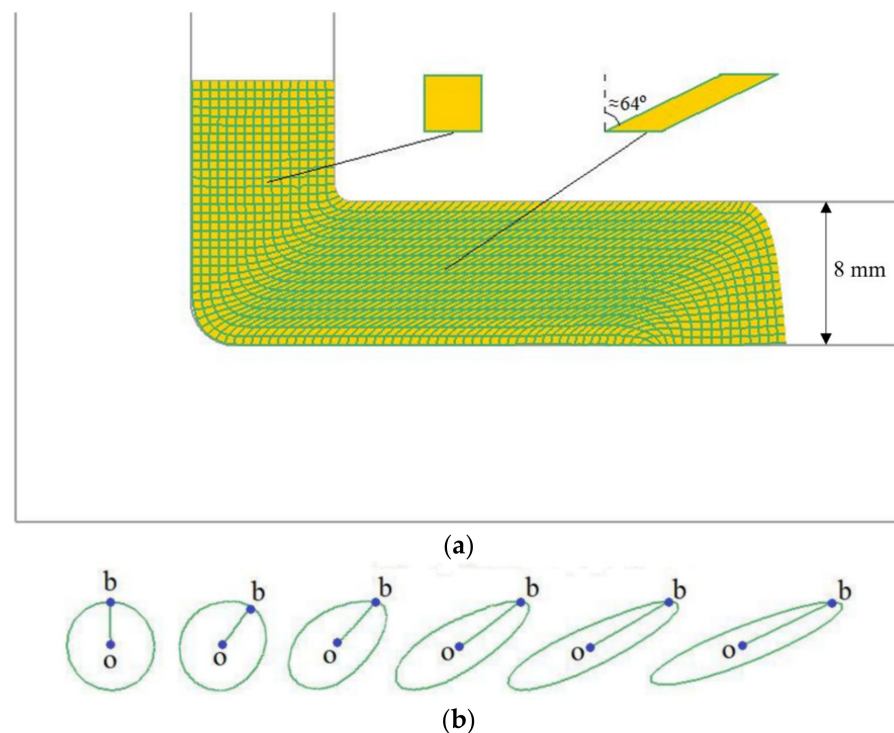


Figure 23. FEM simulation (this work) of simple shear during ECAP (a) and rotation of the axes of the strain ellipsoid when passing through the deformation zone (b).

Simultaneous pure and simple shear combine the advantages of simple shear (rotation of the material as with ECAP) and the advantages of pure shear (compression and elongation of the material as with symmetric rolling). Simultaneous pure and simple shear (Figure 24) corresponds to asymmetric rolling. The square is converted to a parallelogram

and the circle is converted to an ellipse. The thickness “AB” is compressed, and the length “AD” is elongated. The ellipse is rotated (Figure 25) [58].

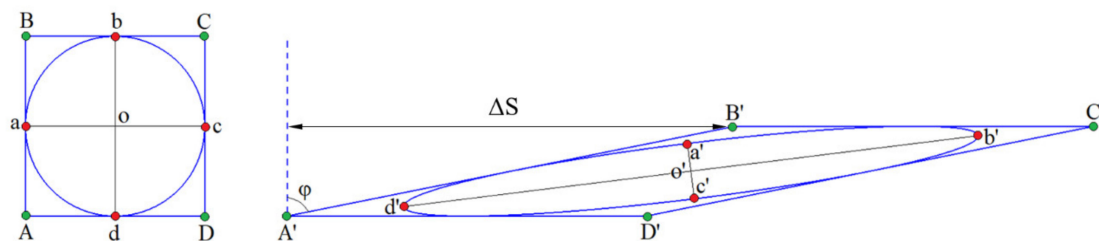


Figure 24. Schematic illustration of simultaneous pure and simple shear during asymmetric rolling.

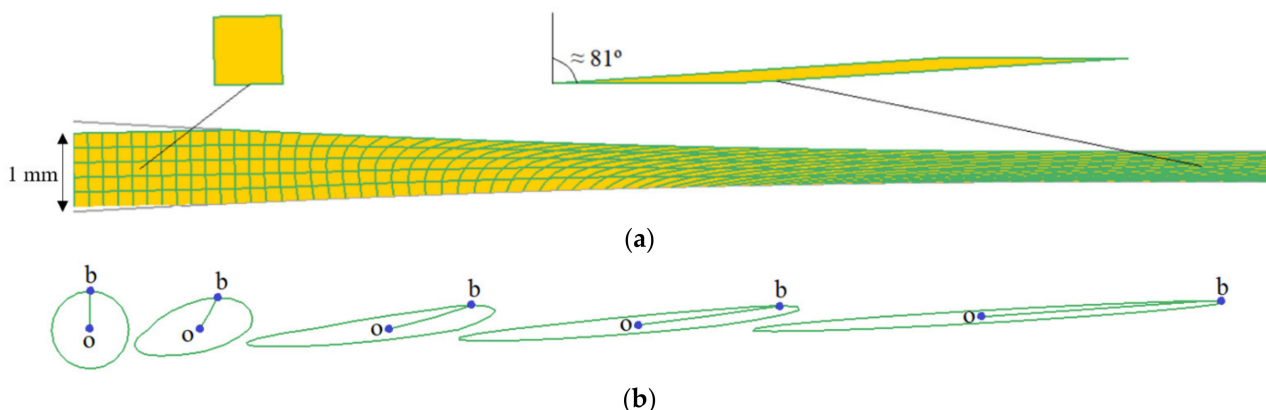


Figure 25. Results of FEM simulation (this work) of simultaneous pure and simple shear during asymmetric rolling (a) and rotation of the axes of the strain ellipsoid when passing through the deformation zone (b) (simulation conditions: room temperature, material AA5083, initial sheet thickness 1.0 mm, thickness reduction 60%, diameters of work rolls 500 mm, Coulomb friction coefficient 0.4, speed of the bottom work roll 43 mm/s, speed of the top work roll 100 mm/s, FEM code DEFORM 2D™).

The equivalent strain  $\bar{\epsilon}$  for asymmetric rolling process can be defined as von Mises strain [23,59–62]:

$$\bar{\epsilon} = \sqrt{\frac{2}{3} e_{ij} e_{ij}} \tag{5}$$

$$\bar{\epsilon} = \sqrt{\frac{2}{9} [(\epsilon_{11} - \epsilon_{22})^2 + (\epsilon_{22} - \epsilon_{33})^2 + (\epsilon_{33} - \epsilon_{11})^2 + 6(\epsilon_{12}^2 + \epsilon_{23}^2 + \epsilon_{31}^2)]} \tag{6}$$

As,  $\epsilon_{11} = \epsilon_{xx}$ ,  $\epsilon_{22} = \epsilon_{yy}$ ,  $\epsilon_{33} = \epsilon_{zz}$ ,  $\epsilon_{12} = \epsilon_{xy}$ ,  $\epsilon_{23} = \epsilon_{yz}$ ,  $\epsilon_{31} = \epsilon_{zx}$ , then

$$\bar{\epsilon} = \sqrt{\frac{2}{9} [(\epsilon_{xx} - \epsilon_{yy})^2 + (\epsilon_{yy} - \epsilon_{zz})^2 + (\epsilon_{zz} - \epsilon_{xx})^2 + 6(\epsilon_{xy}^2 + \epsilon_{yz}^2 + \epsilon_{zx}^2)]} \tag{7}$$

The deformation process during asymmetric rolling can be approximated by a two-dimensional strain state of compressive strain along the normal direction  $z$  ( $\epsilon_{zz}$  and  $\epsilon_{zz} = -\epsilon_{xx}$ ) together with simple shear strain along the rolling direction  $x$  ( $\epsilon_{xz}$ ):

$$\begin{bmatrix} \epsilon_{xx} & 0 & 0 \\ 0 & 0 & 0 \\ 0 & 0 & \epsilon_{zz} = -\epsilon_{xx} \end{bmatrix} + \begin{bmatrix} 0 & 0 & \epsilon_{xz} \\ 0 & 0 & 0 \\ 0 & 0 & 0 \end{bmatrix} = \begin{bmatrix} \epsilon_{xx} & 0 & \epsilon_{xz} \\ 0 & 0 & 0 \\ 0 & 0 & \epsilon_{zz} = -\epsilon_{xx} \end{bmatrix} \tag{8}$$

Then, Equation (7) can be refined as:

$$\bar{\epsilon} = \frac{2}{\sqrt{3}} \sqrt{\epsilon_{xx}^2 + \epsilon_{xz}^2} \tag{9}$$

The compressive strain component and simple shear strain component can be calculated, respectively, as follows:  $\varepsilon_{xx} = \ln \frac{h_0}{h_1}$ ,  $\varepsilon_{xz} = \frac{\gamma_{xz}}{2} = \frac{\gamma}{2}$ , where  $h_0$  is the initial sheet thickness,  $h_1$  is the final sheet thickness. Then, Equation (9) can be refined as:

$$\bar{\varepsilon} = \frac{2}{\sqrt{3}} \sqrt{\left(\ln \frac{h_0}{h_1}\right)^2 + \left(\frac{\gamma}{2}\right)^2} \quad (10)$$

If shear strain  $\gamma = 0$ , then Equation (10) transforms into the well-known equivalent strain  $\bar{\varepsilon}$  for the symmetric rolling process:

$$\bar{\varepsilon} = \frac{2}{\sqrt{3}} \ln \frac{h_0}{h_1} \quad (11)$$

If compressive strain  $\varepsilon_{xx} = 0$ , when  $h_0 = h_1$ , then Equation (10) transforms into the well-known equivalent strain  $\bar{\varepsilon}$  for simple shear:

$$\bar{\varepsilon} = \frac{\gamma}{\sqrt{3}} \quad (12)$$

$$\gamma = tg\varphi \quad (13)$$

where  $\gamma$  is the simple shear strain,  $\varphi$  is the shear angle (see Figure 22). Fueled by advances in severe plastic deformation, there has been much discussion about computing the equivalent strain  $\bar{\varepsilon}$  in simple shear [63]. Since the increment in equivalent strain can be defined via the increment in plastic work, the authors of [63,64] argue for using the von Mises strain (11). On the other hand, Onaka [65] argues that one must use the Hencky relation [66]. The justification given by Onaka is the need to exclude rotations from the deformation gradient tensor in large simple shear deformations. Beygelzimer [67] showed that the equivalent strain of simple shear must be linear in  $\gamma$ . This approach gives evidence in favor of using the von Mises strain (12) for computing the equivalent strain in simple shear.

Saito et al. (1986) [68], Sakai et al. (1988) [69], Cui and Ohori (2000) [15] and Angella et al. (2013) [70] used the following equations for calculation of the equivalent strain  $\bar{\varepsilon}$  and shear strain  $\gamma$  in asymmetric rolling:

$$\bar{\varepsilon} = \frac{2}{\sqrt{3}} \phi \ln \frac{1}{1-r} \quad (14)$$

$$r = 1 - \frac{t_1}{t_0}, \quad \phi = \sqrt{1 + \left\{ \frac{(1-r)^2}{r(2-r)} \tan \theta \right\}^2} \quad (15)$$

$$\gamma = 2\sqrt{\phi^2 - 1} \ln \frac{1}{1-r} \quad (16)$$

where  $t_0, t_1$  are the thickness of the sheet before and after rolling;  $\gamma$  is the shear strain;  $\theta$  is the shear angle.

In 2005, Kang et al. [71] reported that the shear strain component  $\gamma$  imposed by asymmetric rolling with different diameters of the top and bottom work rolls could be calculated by the following equation:

$$\gamma = \frac{1}{\langle D \rangle} \left[ R_1 \cos^{-1} \left( \frac{R_1 - \Delta D/2}{R_1} \right) - R_2 \cos^{-1} \left( \frac{R_2 - \Delta D/2}{R_2} \right) \right] \quad (17)$$

where  $\langle D \rangle = \frac{1}{2}(D_1 + D_2)$ ,  $\Delta D = D_1 - D_2$ ;  $D_1$  is the initial sheet thickness;  $D_2$  is the final sheet thickness;  $R_1$  is the larger radius of the work roll;  $R_2$  is the smaller radius of the work roll.

In 2008, Sidor et al. [60], by using the assumed shear strain  $\gamma$  during asymmetric rolling in accordance with Equation (17), reported that the equivalent von Mises strain could be calculated by the following equation:

$$\bar{\varepsilon} = \frac{\sqrt{2}}{3} \left[ 6 \left[ \ln \left( 1 - \frac{(h_i - h_f)}{h_i} \right) \right]^2 + \frac{6}{(h_i + h_f)^2} \left[ R_1 \cos^{-1} \left( \frac{2R_1 - (h_i - h_f)}{2R_1} \right) - R_2 \cos^{-1} \left( \frac{2R_2 - (h_i - h_f)}{2R_2} \right) \right]^2 \right]^{1/2} \quad (18)$$

where  $h_i$  is the initial sheet thickness,  $h_f$  is the final sheet thickness,  $R_1$  is the larger radius of the work roll,  $R_2$  is the smaller radius of the work roll.

In 2016, Ma et al. [72] reported that the shear strain component  $\gamma$  imposed by asymmetric rolling with the same diameters of work rolls but different angular speeds could be calculated by the following equation:

$$\gamma = \frac{1}{h_i + h_f} R \cos^{-1} \left( 1 - \frac{h_i - h_f}{2R} \right) \left( 1 - \frac{v_2}{v_1} \right) \quad (19)$$

where  $h_i$  is the initial sheet thickness,  $h_f$  is the final sheet thickness,  $R$  is the radius of the work roll,  $v_1$  is the speed of the slower work roll,  $v_2$  is the speed of the faster work roll.

In 2015, Park J.-J. [57] reported that the shear strain component  $\gamma$  imposed by asymmetric rolling with different circumferential speeds could be calculated by the following equation:

$$\gamma = \frac{\Delta s}{t_{ave}} = \frac{(V_{us} - V_{ls})\Delta t}{t_{ave}} = \frac{C(V_{ur} - V_{lr})\Delta t'}{t_{ave}} = \frac{C'L}{t_{ave}} \quad (20)$$

where  $\Delta s$  is the displacement (see Figure 24);  $t_{ave} = \frac{h_0 + h_1}{2}$  is the average thickness of the sheet;  $h_0$  is the initial sheet thickness;  $h_1$  is the final sheet thickness;  $\Delta t$  is the time required for a material point on the fast surface of the sheet to pass through the deformation zone;  $V_{us}$ ,  $V_{ls}$  are the tangential speeds of the upper (faster) and lower (slower) surfaces of the sheet, respectively;  $V_{ur}$ ,  $V_{lr}$  are the tangential speeds of the upper (faster) and lower (slower) work rolls, respectively;  $\Delta t'$  is the time required for a material point on the surface of the fast work roll to pass through the deformation zone;  $L$  is the length of the deformation zone;  $C$  varies from 0 to 0.7 and  $C'$  varies from 0 and 0.5 [57].

Substituting Equation (13) in Equation (10), the equivalent strain  $\bar{\varepsilon}$  depending on the shear angle  $\varphi$  can be found for the asymmetric rolling process. Severe plastic deformation usually corresponds to equivalent strain  $\bar{\varepsilon} \geq 3 \dots 4$ . This requires at least three or four passes of ECAP with a simple shear. This level can be obtained by single-pass asymmetric rolling with simultaneous pure and simple shear, when shear angle  $\varphi$  is no less than  $80^\circ$  (Figure 26) [73].

Taking  $C' = 0.5$  in Equation (20) and simplifying that  $L = \sqrt{R(h_0 - h_1)}$ , and equating Equations (13) and (20), the limiting shear angle  $\varphi_{max}$  can be found:

$$\varphi_{max} = \arctg \frac{\sqrt{R(h_0 - h_1)}}{h_0 + h_1} \quad (21)$$

The influence of initial thickness  $h_0$  of the sheet and thickness reduction per pass  $\varepsilon$  on limiting shear angle  $\varphi$  during asymmetric rolling can be found with Equation (21) (Figure 27). From the graph, it follows that to create a shear angle  $\varphi$  of at least 80 degrees, it is necessary to make the thickness reduction per pass  $\varepsilon \geq 50\%$  when initial sheet thickness  $h_0 = 1$  mm, or  $\varepsilon \geq 70\%$  when  $h_0 = 2$  mm (in all cases, the diameter of work rolls is 300 mm).

The diameters of work rolls (cold rolling mills) at laboratory and industrial scales vary from 50 mm to 600 mm (Figure 28). The influence of diameter  $D$  of work rolls and thickness reduction per pass  $\varepsilon$  on limiting shear angle  $\varphi$  during asymmetric rolling is shown in Figure 29. From the graph, it follows that to create a shear angle  $\varphi$  of at least 80 degrees, it is necessary to make the thickness reduction per pass  $\varepsilon \geq 50\%$  when the diameter of work rolls  $D = 600$  mm, or  $\varepsilon \geq 70\%$  when  $D = 300$  mm (in all cases, the initial thickness of the sheet  $h_0 = 2$  mm).

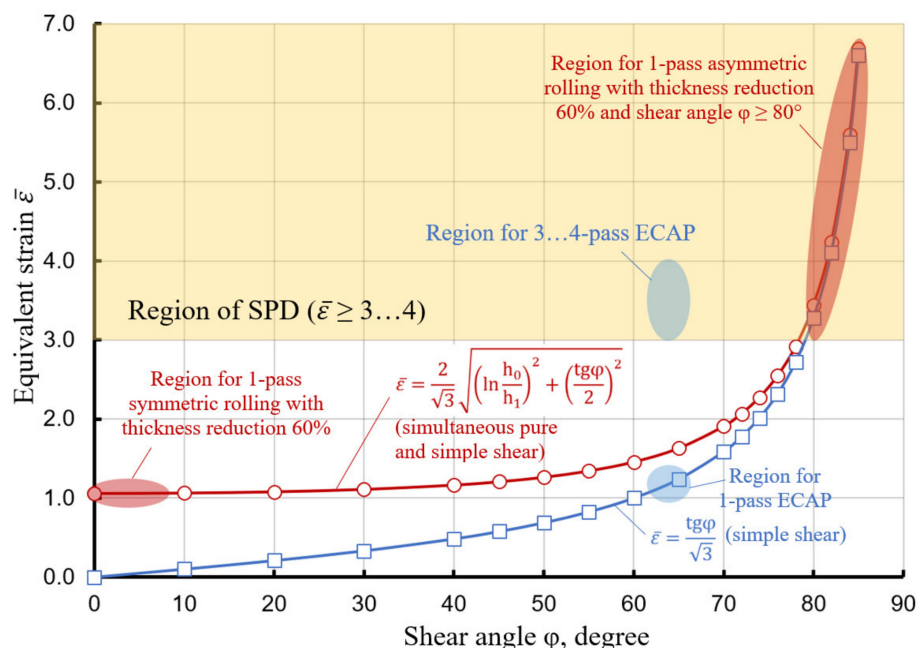


Figure 26. Influence of the shear angle  $\varphi$  on the equivalent strain  $\bar{\epsilon}$  during symmetric rolling, asymmetric rolling and ECAP.

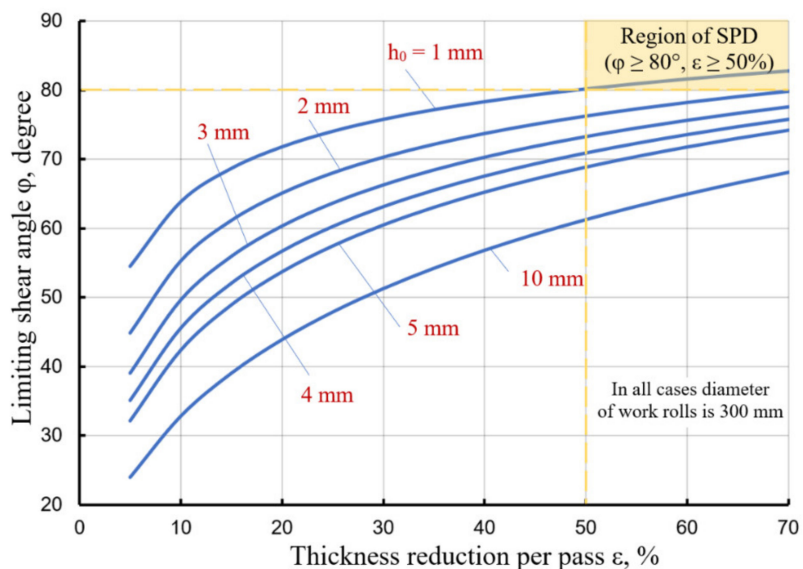


Figure 27. Influence of initial thickness  $h_0$  of the sheet and thickness reduction per pass  $\epsilon$  on limiting shear angle  $\varphi$  during asymmetric rolling.

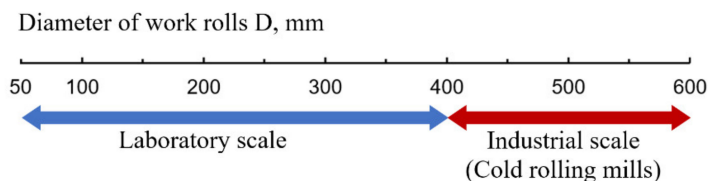
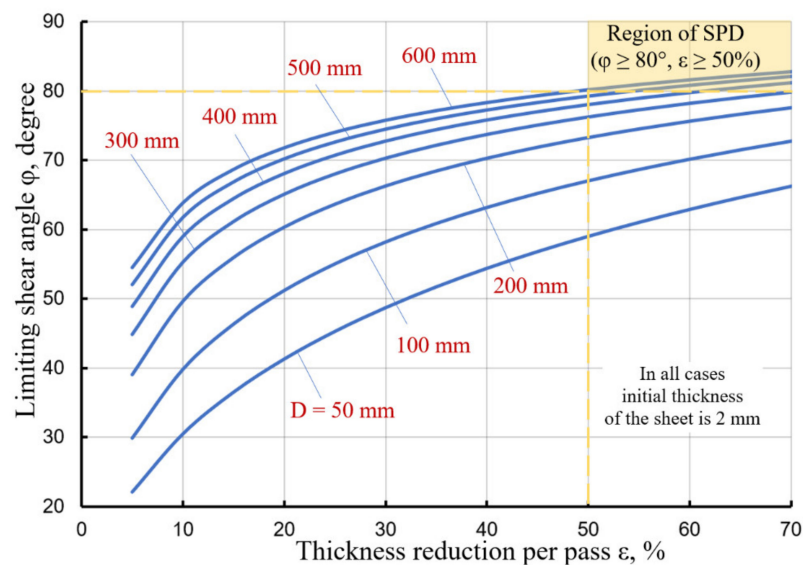


Figure 28. Diameter  $D$  (mm) of work rolls (cold rolling mills) at laboratory and industrial scales.



**Figure 29.** Influence of diameter  $D$  of work rolls and thickness reduction per pass  $\varepsilon$  on limiting shear angle  $\varphi$  during asymmetric rolling.

Hence, a very large equivalent strain  $\bar{\varepsilon} \geq 3 \dots 4$  during asymmetric rolling can be introduced with a large roll diameter ( $D \geq 300$  mm), high thickness reduction per pass ( $\varepsilon \geq 50\%$ ) and thinner initial thickness of the sheet ( $h_0 \leq 2$  mm). In this case, asymmetric rolling should be carried out on dry work rolls without lubrication (with high contact friction) and a high speed ratio of the work rolls ( $S_R = 2 \dots 4$ ).

### 3.4. Temperature Rise

Since asymmetric rolling is performed with high contact friction and high thickness reduction per pass, the temperature increase in the deformation zone can be significant [74–76]. The temperature increase may affect the additional microstructural changes which are related to thermal softening deteriorating the mechanical properties. The model to predict the temperature increase of the sheet during differential speed rolling was proposed in [74]. The temperature increase might be affected by several factors (Table 1). The first factor is the total stored energy which is related to external deformation work. The second factor is the internal energy determined by the mechanical capability of materials, which is defined as the total area beneath the stress–strain curve. The other factors are the energy input caused by frictional heat and the energy loss by non-isothermal conditions. Considering the fact that 90% of the deformation work is converted into heat and 50% of the frictional heat is transferred to the sheet, the energy-based state equation during differential speed rolling is expressed as follows [74]:

$$\rho CV\Delta T = 0.9\sigma\varepsilon V + 0.5m\tau v A\Delta t - Ah\Delta T\Delta t \quad (22)$$

where  $\rho$  is the material density;  $C$  is the heat capacity;  $V$  is the main deformation volume;  $\Delta T$  is the temperature increase in the main deformation volume;  $\sigma$  is the stress;  $\varepsilon$  is the strain;  $m$  is the friction factor;  $\tau$  is the shear stress;  $v$  is the speed of the faster work roll;  $A$  is the contact area between the sheet and the faster work roll;  $\Delta t$  is the deformation time;  $h$  is the heat transfer coefficient.

**Table 1.** Factors and their equations influencing the temperature increase of the sheet during differential speed rolling (based upon the energy-based state equation), reproduced from [74], with permission from Elsevier, 2014.

Factors	Equations
Total stored energy by plastic work	$\rho CV\Delta T$
Internal energy generation by material capability	$0.9\sigma\varepsilon V$
Energy generation by frictional effect	$m\tau v A\Delta t$
Energy loss by non-isothermal conditions	$Ah\Delta T\Delta t$

The temperature increase in the sheet during differential speed rolling can be represented as [74]:

$$\Delta T = \frac{0.9\sigma\varepsilon + 0.5m\tau v \frac{A}{V}\Delta t}{\rho C + \frac{A}{V}h\Delta t} \quad (23)$$

where  $V = Lw\left(\frac{h_0+h_1}{2}\right)$ ;  $A = Lw$ ;  $\Delta t = \frac{L}{v}$ ;  $h_0$  is the initial sheet thickness;  $h_1$  is the final sheet thickness;  $L$  is the length of the deformation zone;  $w$  is the width of the sheet.

Since severe plastic deformation should be performed at relatively low temperatures  $T \leq (0.3 \dots 0.4)T_{melt}$ , the temperature increase in the sheet during differential speed rolling, especially for Mg and Al alloys, must be taken into account.

### 3.5. Deformation Routes

Symmetric rolling can be performed without any kind of rotation of the sheet between each pass. However, in asymmetric rolling, the purpose of imposing high levels of shear strains leads to the idea of rotating the sheet between each rolling pass, taking advantage of the difference in work roll speeds [77]. Several rotation routes can be performed, as shown in Figure 30 [78–81]. By the deformation route UD, the sheet is not rotated before and after each rolling pass, while in the other three cases it is rotated by 180° degrees. By the route RD, the rotation axis is the rolling direction, by the route TD it is the transverse direction and by the route ND it is the normal direction. From the observation of the possible reversal routes, it becomes clear that the UD and TD routes do not impose any reversal of strains on the sheet's surface, whereas RD and ND impose strain reversal. In the literature, the TD route is one of the most commonly used, but when studying the asymmetric rolling process, S.H. Lee and D.N. Lee [78] observed textures closer to the ideal "shear" components on specimens processed by the RD and ND reversing routes. Using FEM simulations, Kim and Lee [82] studied the influence of shear strain evolution during symmetric and asymmetric rolling. They found that in symmetric rolling, the sheet undergoes positive and negative shear strains, before and after the neutral point, respectively [82,83]. However, during asymmetric rolling, shear strains are positive. By using the shear strain history, determined for symmetric and asymmetric rolling, Kim and Lee calculated the resulting crystallographic textures. They found that the ideal shear textures were closely related to the shear strain reversal. In order to understand the influence of the deformation route, it is necessary to examine the shear patterns. These patterns are illustrated schematically in the form of the dominant directions of shear for routes UD, TD, RD and ND. It is apparent from Figure 30 that the shear patterns are significantly different between UD, TD and RD, ND deformation routes [84]. Routes UD and TD repeat shear on the same plane. By contrast, routes RD and ND have two shear planes intersecting at the shear angle. Y.G. Ko and K. Hamad [85], for AZ31 Mg alloy, experimentally showed that the RD route is the most effective in grain refinement, yielding equiaxed grains with an average size of 1.2 μm, while routes UD and TD yielded elongated grains with average sizes of 1.4 and 2.1 μm, respectively (Figure 31). Route ND, in turn, led to equiaxed fine grains (1.3 μm), but the through thickness homogeneity achieved by the ND route was less than that achieved by the RD. The coarser-grained microstructures

obtained for the sheets deformed by the UD and TD routes led to lower yield strengths compared to those deformed by the RD and ND routes [85].

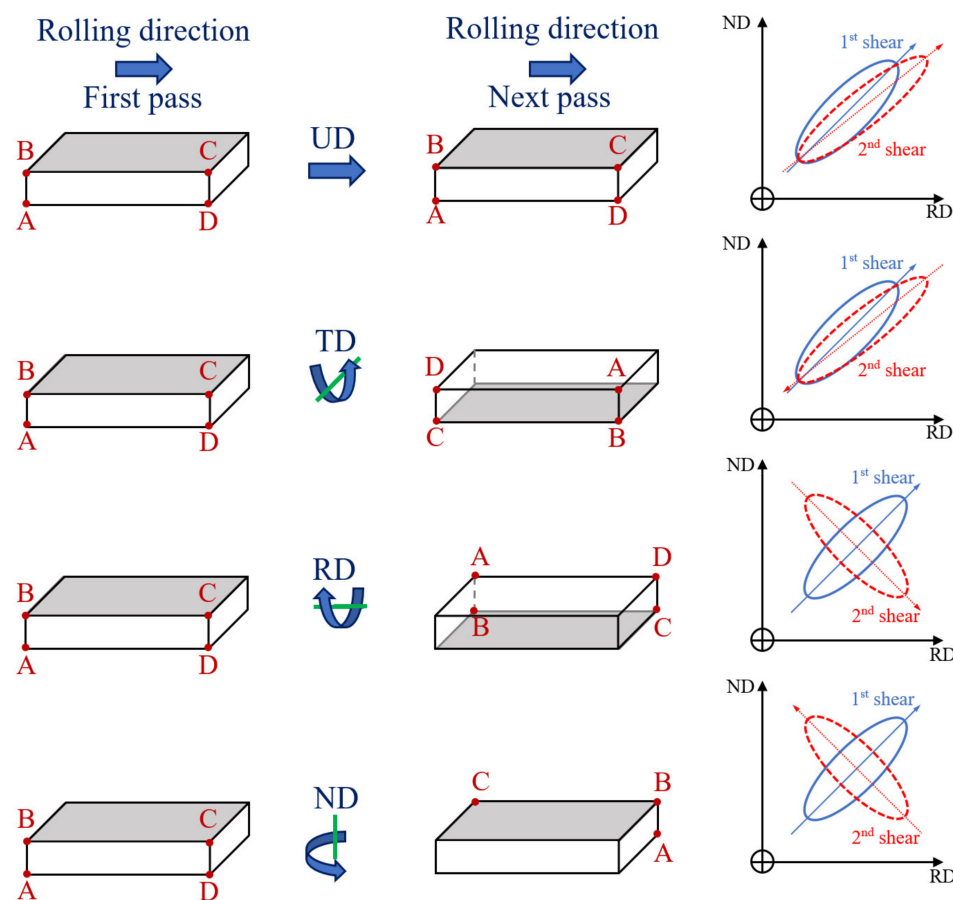


**Figure 30.** Schematic illustration of deformation routes and shear directions during asymmetric rolling. In UD rolling, rolling direction is not changed, whereas in TD, RD and ND rolling, the sheet is rotated through 180° about TD, RD and ND axes, respectively, for each pass. Reprinted from [84].

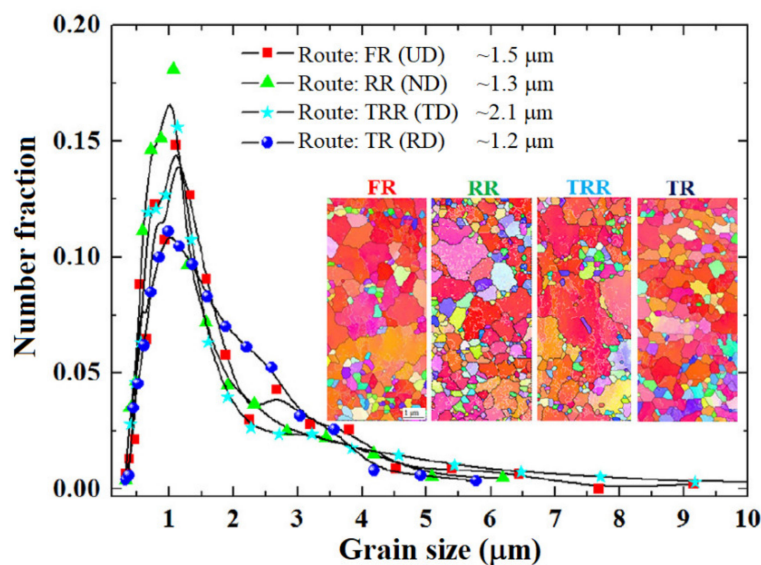


**Figure 31.** Grain size distributions and average grain sizes of the AZ31 Mg alloy samples deformed by differential speed rolling using the different deformation routes (thickness reduction from 4 mm to 1 mm by two passes, speed ratio  $S_R = 4.0$ ), reproduced from [85], with permission from Elsevier, 2018.

Asymmetric rolling can give rise to severe plastic shear strains and in turn shear deformation textures through the sheet thickness. The ideal shear deformation texture of FCC metals can be approximated by the  $\langle 111 \rangle // \text{ND}$  and  $\{001\} \langle 110 \rangle$  orientations, among which the former improves the deep drawability. The ideal shear texture could not be obtained by using unidirectional asymmetric rolling, but only by using RD or ND reversing deformation routes [82,83].

One of the most important parameters in asymmetric rolling is the thickness reduction per pass [77]. When combined with a difference in work roll speeds, an increase in thickness reduction per pass imposes higher levels of shear strain on the sheet surface and, under the appropriate conditions, it is essential to achieve the total propagation of those shear strains along the sheet's thickness. Kim and Lee [82] studied the influence of the reduction per pass on the shear texture formation. They found that high values of this parameter were necessary to achieve shear textures. Low thickness reductions per pass led to plane strain textures, similar to those found with conventional rolling. At the same time, the thickness reduction per pass has a nonlinear effect on grain refinement. Lee and Lee [79,86], from the experimental results, concluded that a 5% or 50% reduction per pass gave rise to finer grains with a higher fraction of high angle boundaries than reductions of 10, 20 and 30% per pass (Figure 32). Figure 33a shows EBSD mappings of AA1050 sheets asymmetrically rolled by 93%. Uniformly distributed high-angle boundary structures developed in the sheets rolled with 5% and 50% reductions per pass. It can be seen that the 5% and 50% sheets have higher fractions of high-angle boundaries over  $15^\circ$  and finer grain sizes, as shown in Figure 32. The grain size decreased from the initial size of about  $100 \mu\text{m}$  to  $1.4\text{--}1.8 \mu\text{m}$  [79].

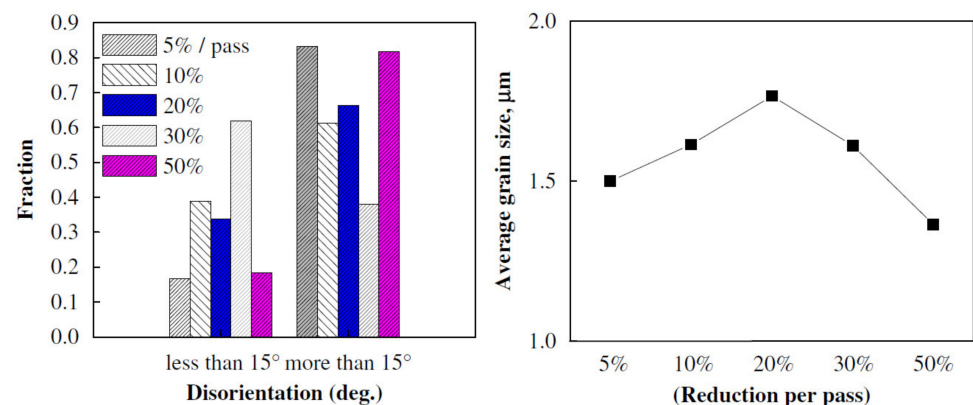


**Figure 32.** Disorientation distributions and average grain sizes in AA1050 sheets asymmetrically rolled by 93% after annealing at  $195^\circ\text{C}$  for 60 min (thickness reduction from 4.2 mm to 0.3 mm, speed ratio  $S_R \approx 2.0$  due to different diameters of work rolls of 248 mm and 128 mm), reproduced from [79], with permission from Elsevier, 2008.

The equivalent strain  $\bar{\epsilon}$  in the surface layer of the rolled sheet is a function of friction coefficient  $\mu$  and the geometric shape factor  $L/t_{ave}$  (where  $L = \sqrt{R(h_0 - h_1)}$  is the length of the deformation zone;  $t_{ave} = (h_0 + h_1)/2$  is the average thickness of the sheet;  $h_0$  is the initial sheet thickness;  $h_1$  is the final sheet thickness) [79]. During rolling with high contact friction, the equivalent strain  $\bar{\epsilon}$  is the highest when the geometric shape factor  $L/t_{ave}$  is very small or, on the contrary, very large (Figure 33b) [79]. For a given thickness reduction, the equivalent strain  $\bar{\epsilon}$  is proportional to shear strains because the normal strains are the same, as can be seen in Equation (6). Therefore, the minimum equivalent strain  $\bar{\epsilon}$  in Figure 33b corresponds to the minimum shear strain at some value of geometric shape factor  $L/t_{ave}$ . The geometric shape factors  $L/t_{ave}$  at 5% and 50% thickness reductions per pass in [79,86] could be on the left and right sides of the minimum equivalent strain  $\bar{\epsilon}$  or the minimum shear strain, respectively. Thus, the reason why a 5% or 50% thickness reduction per pass

gave rise to finer grains with a higher fraction of high-angle boundaries than thickness reductions of 10, 20 and 30% per pass can be explained.

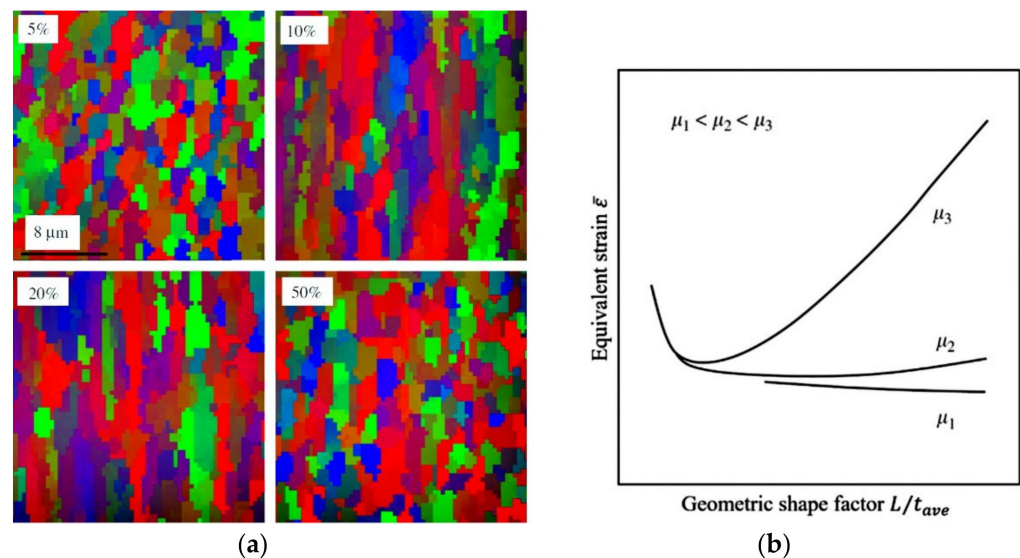


**Figure 33.** (a) EBSD mapping along rolling plane of AA1050 sheets asymmetrically rolled by 93% after annealing at 195 °C for 60 min (thickness reduction from 4.2 mm to 0.3 mm, speed ratio  $S_R \approx 2.0$  due to different diameters of work rolls of 248 mm and 128 mm). (b) Schematic representation of equivalent strain  $\bar{\epsilon}$  in the surface layer against geometric shape factor  $L/t_{ave}$  at different friction coefficients  $\mu$ , reproduced from [79], with permission from Elsevier, 2008.

#### 4. Asymmetric (Hot, Warm, Cold) Rolling of Mg Alloys

Magnesium alloys (especially those containing Al and Zn additions—so-called AZ series) are in many fields superior to aluminum alloys (e.g., they possess a lower density and thus a better specific strength). However, their problematic formability requires consideration [62]. Over the last 20 years, a number of scientific works have been devoted to a fabrication of Mg alloy sheets with a good drawability. It was proposed that the main reason for the very poor cold formability and high mechanical anisotropy is an induction of a strong  $\{0\ 0\ 0\ 1\}$  basal texture in conventional plastic-forming processing due to a limited number of slip systems in the hexagonal close-packed (hcp) crystal structure [62]. The results of an extensive study on various Mg alloys (Tables 2–4 and Figure 34) showed that the (hot, warm, cold) differential speed rolling has a great impact on the intensity of the basal texture, grain size and plasticity of these materials. It was established that increasing the shear strain by raising the roll speed ratio  $S_R$  leads to weakening of the basal texture through facilitating the activation of prismatic slip during deformation. The basal texture weakening effect at high speed ratios is attributed to extensive tension twinning that occurs in the basal-oriented matrix. Consequently, the asymmetrically rolled Mg alloy sheets are characterized not only by more isotropic properties but also by the enhanced plasticity combined with exceptionally high strength that is related to the simultaneous structure refinement. Therefore, the differential speed rolling process is considered to be one of the most efficient techniques for processing these materials.

Table 2. Experimental data related to asymmetric hot rolling of Mg alloys.

Material	Initial/Final Sheet Thickness, mm	Top/Bottom Work Roll Diameters, mm	Speed Ratio $S_R$	Total Reduction/Number of Passes	$T$ , °C	Final Grain Size, $\mu\text{m}$	YS, MPa	UTS, MPa	EL, %	Ref.
Pure Mg	10/2.5	165/110	1.5	75%/2	350	6.74	-	-	-	[87]
Pure Mg	10/2.5	-	1.5	75%/2	350	6.7	-	-	-	[88]
Mg-3%Ca	2.0/0.7	-	2.0	65%/2	300	5.81	162.1	-	2.4	[89]
ZK60	1.0/0.55	-	1.5	45%/4	300	-	252	322	7.7	[90]
AZ31	6.0/2.0	700/600	1.25	67%/2	300	-	188	272	21	[91]
AZ31	4.3/1.8	220/220	3	58%/2	300	15	185	265	17.5	[92]
AZ31	4.3/1.8	220/220	3	58%/2	350	16	180	265	19	[92]
AZ31	6.0/1.0	-	1.2	83.3%/6	350	10.3	145	240	28.5	[93]
AZ31	1.0/0.85	-	1.1	15%/1	300	-	241	289	13.6	[94]
AZ91	3.5/2.98	150/150	Single roll drive	15%/1	400	86.7	-	255.5	3.7	[95]
	4.0/1.5	-	1.167	63%/1	300	11	-	-	-	
	4.0/1.5	-	1.167	63%/2	300	9	-	-	-	
AZ31	4.0/1.5	-	1.167	63%/4	300	10	-	-	-	[96]
	4.0/1.5	-	1.167	63%/6	300	10	-	-	-	
	4.0/1.5	-	1.167	63%/8	300	12	-	-	-	
	4.0/1.5	-	1.167	63%/10	300	12	-	-	-	
ZK60	1.0/0.55	-	1.2	45%/4	300	-	246	331	6.1	[97]
	1.0/0.55	-	1.5	45%/4	300	-	253	323	7.7	
AZ31B	4.0/2.0	-	1.167	50%/6	430	-	-	-	-	
	2.0/1.0	-	1.167	50%/8	300	-	145.5	259.2	25.5	[98–100]
AM31	1.0/0.5	-	1.2	50%/2	300	5.6	195	265	17.5	[101]
	1.0/0.5	-	1.5	50%/2	300	4.9	181	257	16.9	[101]
AZ31	10/1.5	-	1.05	85%/8	350	5.0	-	-	-	[102]
AZ80	5.0/1.0	-	1.36	80%/4	430	7.0	182	330	24.6	[103]
AZ31	2.0/0.6	-	3.0	70%/1	350	3.8	158	260	18	[16]
AM31	1.0/0.55	-	1.2	45%/2	300	6.9	222	283	18.3	[104]
	1.0/0.55	-	1.5	45%/2	300	4.9	217	259	17.6	[104]
AZ91	2.0/0.5	-	2.0	75%/2	400	1~2	310	-	7 830 *	[105]
AZ31B	4.0/2.0	160/160	1.167	50%/6	430	-	-	-	-	[106]
	2.0/1.0	160/160	1.167	50%/8	300	12.3	-	-	-	[106]
Mg-9.25Zn-1.66Y	2.0/0.61	-	2	69.5%/2	400	1~2	342	-	4.2	[107]
	2.0/0.63	-	3	68.5%/2	400	0.5~1.0	337	-	10.7	[107]
Mg-4Y-3RE	5.0/1.0	-	1.36	80%/4	550	-	-	-	-	[108]
Mg-13Zn-1.55Y	2.0/0.6	-	3.0	70%/2	400	1~2	-	-	1021 **	[109]
AZ31	5.3/2.25	190/128	1.5	57.5%/1	500	-	-	-	-	[110]
	6.5/1.0	190/128	1.5	84.6%/9	500	-	-	-	-	[110]

\* Superplasticity at 300 °C and  $1 \times 10^{-3} \text{ s}^{-1}$ ; \*\* superplasticity at 250 °C and  $1 \times 10^{-3} \text{ s}^{-1}$ .

**Table 3.** Experimental data related to asymmetric warm rolling of Mg alloys.

Material	Initial/Final Sheet Thickness, mm	Top/Bottom Work Roll Diameters, mm	Speed Ratio $S_R$	Total Reduction/Number of Passes	$T_r$ , °C	Final Grain Size, $\mu\text{m}$	YS, MPa	UTS, MPa	EL, %	Ref.
Pure Mg	10/2.5	165/110	1.5	75%/2	200	3.95	-	-	-	[87]
AZ31	2.0/0.6	300/300	3.0	70%/1	200	3.0	-	-	-	[111]
Pure Mg	10/2.5	-	1.5	75%/2	200	4.0	-	-	-	[88]
AZ31B	2.0/1.6	280/280	1.5	20%/1	200	-	-	-	-	[112]
AZ31	1.6/0.4	70/60	1.17	75%/12	150	1.47	-	-	-	[113]
Mg-1Gd	1.6/0.4	70/60	1.17	75%/12	150	1.7	-	-	-	[113]
	4.3/2.8	220/220	3	35%/1	200	9.2	240	280	14	
	4.3/1.8	220/220	3	58%/2	200	5.4	265	320	8.5	
AZ31	4.3/2.8	220/220	3	35%/1	250	12.1	180	265	17.5	[92]
	4.3/1.8	220/220	3	58%/2	250	9.1	185	265	15.5	
AZ31	2.0/1.7	-	3.0	15%/1	150	-	-	-	-	[114]
	2.0/1.6	400/400	1.1	20%/1	240	6.3	236.9	295.5	12.2	
	2.0/1.6	400/400	1.2	20%/1	240	4.3	241.5	296.3	13.8	
AZ31	2.0/1.6	400/400	1.5	20%/1	240	3.5	233.8	288.5	6.8	[115]
	2.0/1.6	400/400	2	20%/1	240	6.1	209.6	281.8	16	
	2.0/1.6	400/400	3	20%/1	240	5.9	201	281.8	16.7	
	1.0/0.85	-	1.1	15%/1	200	-	242	295	18.5	
AZ31	1.0/0.85	-	1.1	15%/1	250	-	237	290	17.3	[94]
AZ31	2.0/0.68	300/300	2.0	66%/2	150	0.6	382	401	6.8	[116]
AZ31	2.0/0.51	400/400	2.0	74.5%/3	200	2.3	275.5	309.7	22.1	[117]
AZ31	2.0/0.6	300/300	3.0	70%/1	150	1.4	-	-	-	[17]
AZ31	2.0/0.9	90/90	3.0	55%/1	150	1.0	-	-	-	[118]
	2.0/0.6	-	3	70%/1	140	1.4	294	317	5	
	2.0/0.6	-	3	70%/1	160	1.5	275	320	24	
AZ31	2.0/0.6	-	3	70%/1	200	2.9	188	274	23	[16]
	2.0/0.6	-	3	70%/1	250	3	180	268	18	
AZ31	4.0/2.0	220/220	3.0	50%/2	180	3.3	198	228	7.1	[119]
AZ61	2.0/0.6	-	3.0	70%/1	200	0.3–0.5	-	-	850 *	[120]
AZ31	4.0/2.0	220/220	4.0	50%/2	150	1.2	295	-	21	[85]
ZK60	2.0/0.6	-	3.0	70%/1	200	1–2	286	338	30 1000 **	[18]

\* Superplasticity at 250 °C and  $3 \times 10^{-4} \text{ s}^{-1}$ ; \*\* superplasticity at 280 °C and  $1 \times 10^{-3} \text{ s}^{-1}$ .

**Table 4.** Experimental data related to asymmetric cold rolling of Mg alloys.

Material	Initial/Final Sheet Thickness, mm	Top/Bottom Work Roll Diameters, mm	Speed Ratio $S_R$	Total Reduction/Number of Passes	$T_r$ , °C	Final Grain Size, $\mu\text{m}$	YS, MPa	UTS, MPa	EL, %	Ref.
Pure Mg	10/2.5	165/110	1.5	75%/2	20	2.11	-	-	-	[87]
Pure Mg	10/2.5	-	1.5	75%/2	20	2.3	-	-	-	[88]
AZ91	3.5/2.98	-	Single roll drive	15%/1	20	98	-	-	-	[121]
ZK60	2.0/0.64	400/400	3.0	68%/1	20 *	1.0	-	-	-	[122]

\* Cold sheet was fed into hot (200 °C) rolls.



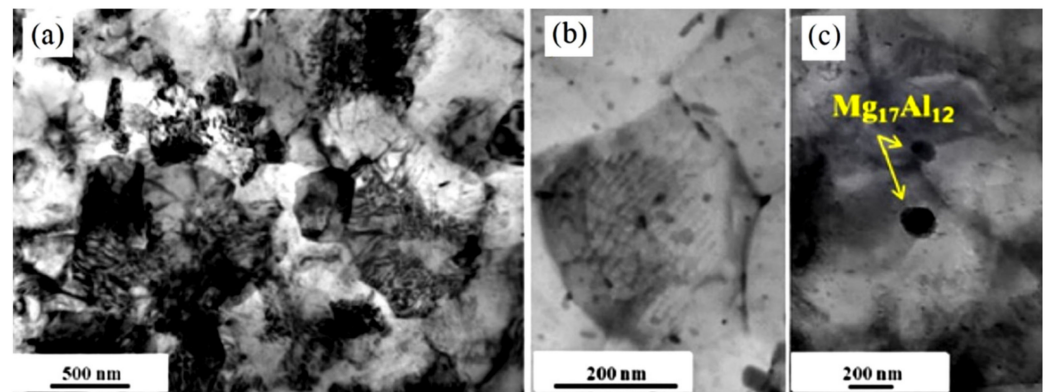


**Figure 35.** (a) TEM micrograph of AZ31 sheet obtained after high-ratio differential speed rolling ( $S_R = 2$ ) at 150 °C followed by immediate water quenching. (b) Al–Mn and (c)  $\beta$ - $Mg_{17}Al_{12}$  particles in the matrix, reproduced from [116], with permission from Elsevier, 2011.

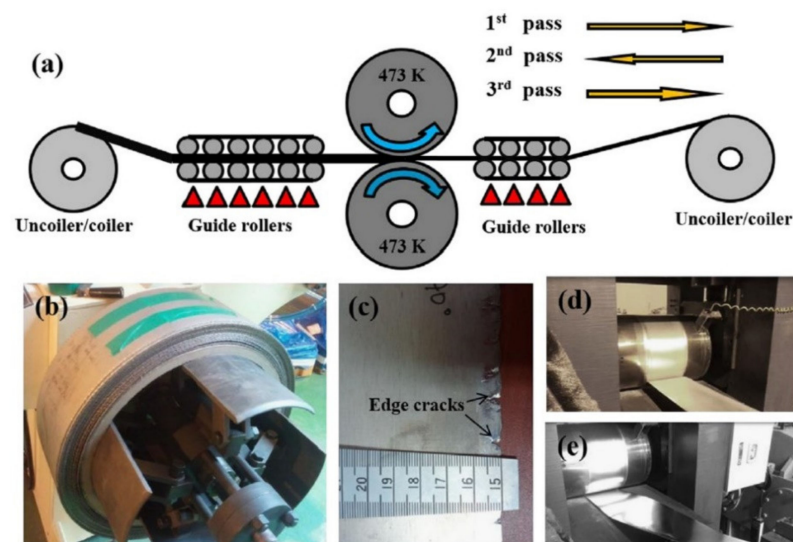


**Figure 36.** (a) The layout of the continuous HRDSR mill. (b) The appearance of the HRDSR-processed sheets in coil form. (c) The appearance of the HRDSR-processed sheets. Snap shots of the sheets coming out of the rollers during the second pass under (d) HRDSR and (e) conventional rolling conditions, reproduced from [117], with permission from Elsevier, 2014.

### 5. Asymmetric (Hot, Warm, Cold, Cryo) Rolling of Al Alloys

Aluminum and aluminum alloys are well known for their high mechanical property anisotropy (a so-called earing behavior) upon a deep drawing process [62]. It was recognized that the main determinant of such behavior is a  $\{100\}\langle 100\rangle$  cubic crystallographic texture formed in a fully annealed state [62]. On the other hand, it was proposed by Lequeu and Jonas [123] that formation of the undesired  $\{100\}\langle 100\rangle$  recrystallization texture component may be prominently inhibited through an application of shear strain prior to a heat treatment. Therefore, a number of works have been devoted to the development of asymmetric rolling-based processing techniques that allow for the fabrication of aluminum alloy sheets with enhanced formability [62]. Engler et al. [124] reported that the most efficient method of formability improvement is to introduce  $\{111\}$  textures (composed of crystallographic orientations that are characterized by  $\{111\}$  crystallographic planes parallel to a rolling plane). Since these orientations are normally found in BCC metals and alloys (and are responsible for an excellent drawability of low-carbon steels), in the case of FCC metals, they may be produced only by shear strain. Jin and Lloyd [125] proved that the recrystallization texture of AA5754 aluminum alloy is randomized (the  $\{001\}\langle 100\rangle$

component is prominently reduced), when a high-ratio differential speed rolling ( $S_R = 1.5$  and  $S_R = 2$ ) is applied before the annealing treatment. The {111} shear strain texture is maintained in the material after annealing that allows for the lowering the so-called planar anisotropy (that characterizes an alteration of mechanical properties in different directions lying in the rolling plane). Analogous results were also obtained by Sakai et al. [39], who showed that 5052 aluminum alloy cold deformed with a 75% thickness reduction in a two-pass asymmetric rolling process followed by recrystallization annealing at a temperature of 310–460 °C exhibits almost perfectly isotropic mechanical behavior (values of the planar anisotropy coefficient were reduced to nearly zero) [62].

Results of an extensive study on various Al alloys (Tables 5–8 and Figure 37) showed that (hot, warm, cold, cryo) differential speed rolling has a great impact on the grain size and mechanical properties of these materials.

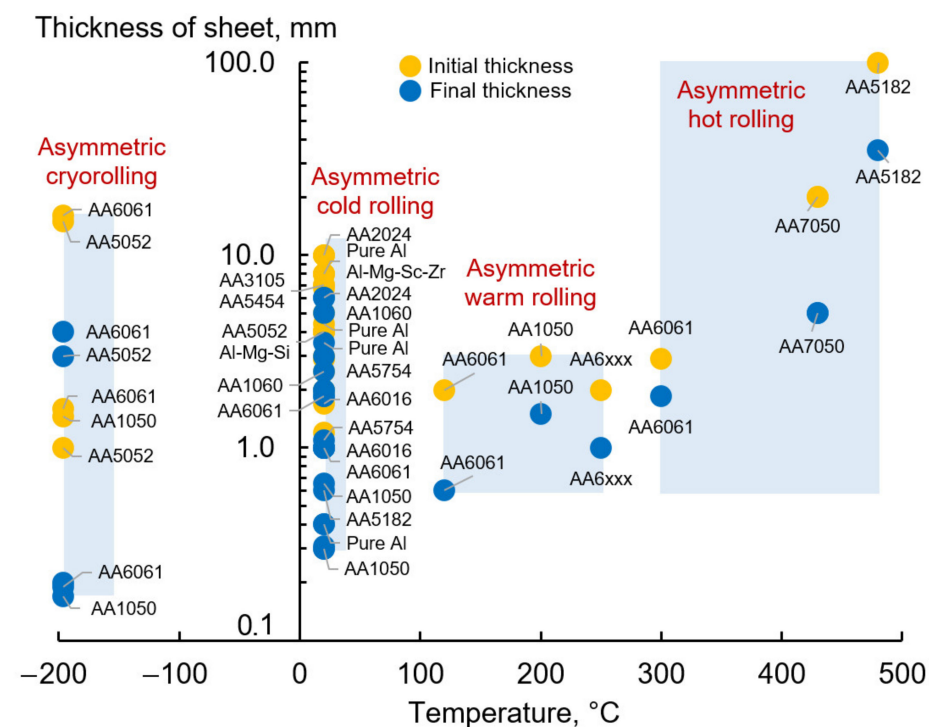


Figure 37. Different Al alloys, which were processed by asymmetric (hot, warm, cold) rolling (based on data from Tables 5–8).

**Table 5.** Experimental data related to asymmetric hot rolling of Al alloys.

Material	Initial/Final Sheet Thickness, mm	Top/Bottom Work Roll Diameters, mm	Speed Ratio $S_R$	Total Reduction/Number of Passes	$T_r$ , °C	Final Grain Size, $\mu\text{m}$	YS, MPa	UTS, MPa	EL, %	Ref.
AA5182	100/35	450/480	1.07	65%/6	480	-	113.3	272.7	30.5	[55]
							112.8	271.8	31.2	
							113.7	273.3	30.1	
							113.3	273.3	29.2	
AA7050	100/35	400/480	1.2	65%/6	480	-	112	272.2	30.5	[126]
							115.7	275	28.7	
AA7050	20/5	400/400	1.25	75%/4	430	-	445	568	22.8	[72]
							459	543	11.6	
							475	539	5.2	
							467	548	12.2	
AA7050	20/5	400/400	1.25	75%/2	430	14.6	467	548	12.4	[72]
							468	534	9.6	
							428	540	13.2	
							466	550	16.4	
AA6061	20/5	400/400	1.25	75%/4	430	12.7	434	559	14.4	[127]
							411	548	18	
							478	553	17.6	
							499	564	18	
AA6061	2.9/1.85	180/180	1.5	36%/1	300	-	474	562	18	[127]
							-	-	-	

**Table 6.** Experimental data related to asymmetric warm rolling of Al alloys.

Material	Initial/Final Sheet Thickness, mm	Top/Bottom Work Roll Diameters, mm	Speed Ratio $S_R$	Total Reduction/Number of Passes	$T_r$ , °C	Final Grain Size, $\mu\text{m}$	YS, MPa	UTS, MPa	EL, %	Ref.
AA1050	3.0/1.5	130/130	1.5	50%/1	200	-	-	-	-	[37]
AA6061	2.0/0.6	300/300	3.0	70%/1	120	0.37	455	489	7.4	[19]
AA6xxx	2.0/1.0	-	2.0	30%/2	250	-	134	261	37	[128]

Table 7. Experimental data related to asymmetric cold rolling of Al alloys.

Material	Initial/Final Sheet Thickness, mm	Top/Bottom Work Roll Diameters, mm	Speed Ratio $S_R$	Total Reduction/Number of Passes	$T_r$ , °C	Final Grain Size, $\mu\text{m}$	YS, MPa	UTS, MPa	EL, %	Ref.
AA5xxx	2.0/1.0	-	2.0	50%/2	20	-	-	306	33.6	[129]
AA1060	5.0/2.5	100/100	1.02	50%/1	20	12.49	131.6	141	8.88	[130]
AA2024	10/6	150/150	-	40%/-	20	-	-	-	-	[131,132]
AA3105	7/-	-	1.18	-	20	-	-	-	-	[133]
AA5052	4.0/1.0	220/220	4.0	75%/4	20	0.7	380	390	4.2	[134]
AA5052	4.0/1.0	220/220	4.0	75%/2	20	0.5	-	-	-	[22]
AA5052	4.0/1.0	220/220	4.0	75%/4	20	0.7	380	-	4	[135]
AA5182	1.2/0.6	180/180	3.0	50%/2	20	-	-	-	-	[136]
	3.0/2.25	180/180	1.36	25%/1	20	33	230	380	13.5	
AA5182	3.0/1.5	180/180	1.36	50%/2	20	20	280	410	10.5	[137]
	3.0/1.0	180/180	1.36	66%/4	20	-	310	420	10	
	3.0/0.3	180/180	1.36	90%/6	20	0.3	370	450	7.5	
	6.7/-	295/295	1.5	33%/1	20	17.7	-	280	-	
AA5454	6.7/-	295/295	2	33%/1	20	17.5	235	280	-	[138]
	6.7/-	295/295	1.5	44%/1	20	18	-	293	-	
	6.7/-	295/295	2	44%/1	20	17.5	253	291	-	
AA5754	-	161.5/161.5	2.0	-	20	-	-	-	-	[139]
AA5754	2.5/1.1	161.5/161.5	2.0	56%/2	20	-	-	-	-	[125]
AA6016	1.7/1.0	-	1.5	41%/2	20	-	-	-	-	[140]
AA6061	4.0/1.0	-	4.0	75%/4	20	0.8	322	-	-	[141]
AA6061	2.9/1.85	180/180	1.5	36%/1	20	4.0	-	-	-	[130,142]
AA6111	-	161.5/161.5	4.0	50%/2	20	30	-	-	-	[143]
Pure Al	2.0/1.0	126/157.5	1.25	50%/1	20	-	-	-	-	[82]
	2.0/1.0	126/189	1.5	50%/1	20	-	-	-	-	
AA1050	2.92/0.3	300/300	1.5	90%/4	20	-	-	-	-	[144]
Pure Al	8.0/3.0	180/180	3.0	62.5%/6	20	-	108	121	-	[145]
AA1050	7.0/3.5	-	2.0	50%/8	20	-	-	-	-	[146]
AA6016	1.22/1.0	310/460	1.5	18%/1	20	-	-	-	-	[147]
AA1050	8.0/0.65	180/180	1.36	92%/15	20	-	-	-	-	[148]
	8.0/0.65	180/180	1.36	92%/4	20	-	-	-	-	
Pure Al	4.0/0.4	130/130	-	90%/22	20	1.0	250	-	4	[149]
Pure Al	4.0/1.2	130/130	1.5	70%/11	20	0.5	-	-	-	[59]
AA1050	4.4/0.3	248/128	1.94	93%/4	20	1.4	-	-	-	[79,86]
	4.4/0.3	248/128	1.94	93%/52	20	1.5	-	-	-	
Al-Mg-Sc-Zr	8.0/2.0	100/100	1.3	75%/10	20	1.5	-	-	3200 *	[150]
Al-Mg-Mn-Sc-Zr	8.0/2.0	100/100	1.5	75%/10	20	1.1	-	-	3170 *	[151]
Al-Mg-Si	4.0/1.0	-	4.0	75%/4	20	-	-	312	7.4	[152]

\* Superplasticity at 500 °C and  $5 \times 10^{-2} \text{ s}^{-1}$ .

Table 8. Experimental data related to asymmetric cryorolling of Al alloys.

Material	Initial/Final Sheet Thickness, mm	Top/Bottom Work Roll Diameters, mm	Speed Ratio $S_R$	Total Reduction/Number of Passes	$T$ , °C	Final Grain Size, $\mu\text{m}$	YS, MPa	UTS, MPa	EL, %	Ref.
AA1050	1.45/0.17	-	1.1	88%/7	-196	0.36	154	160	-	[24,153]
	1.45/0.17	-	1.2	88%/7	-196	-	159	179	-	
	1.45/0.17	-	1.3	88%/7	-196	-	160	182	-	
	1.45/0.17	-	1.4	88%/7	-196	0.21	162	196	-	
AA6061	1.5/0.19	120/120	1.1	87.3%/7	-196	0.235	-	235	-	[25]
AA6061	1.5/0.19	-	1.1	87.3%/7	-196	-	-	-	-	[26]
AA5052	1.0/0.2	-	1.4	80%/3	-196	0.35	-	343	3.3	[154]
AA5052	15/3	130/130	1.2	80%/15	-196	-	267	295	6.8	[155]
	15/3	130/130	1.5	80%/15	-196	-	252	286	9.2	
AA6061	16/4	-	1.5	75%/13	-196	-	-	-	-	[156]

In 2009, Jiang et al. [149] showed that ultrafine-grained pure Al with an average grain size of  $\sim 1 \mu\text{m}$  (Figure 38a) could be prepared by asymmetric cold rolling. The sheets were rolled with a total thickness reduction of 90% from 4 mm to 0.4 mm after 22 rolling passes. The grains of the material were nearly equiaxed and the microstructure was homogeneous. Moreover, the high-angle grain boundaries were predominant. The fraction of high-angle grain boundaries ( $>15^\circ$ ) was about 50%. Before rolling, the original pure Al was of very low yield stress ( $\sim 100 \text{ MPa}$ ) and high ductility ( $\sim 17\%$ ). The yield strength of asymmetrically rolled Al increased to 250 MPa, but the corresponding elongation decreased to 4% [149].

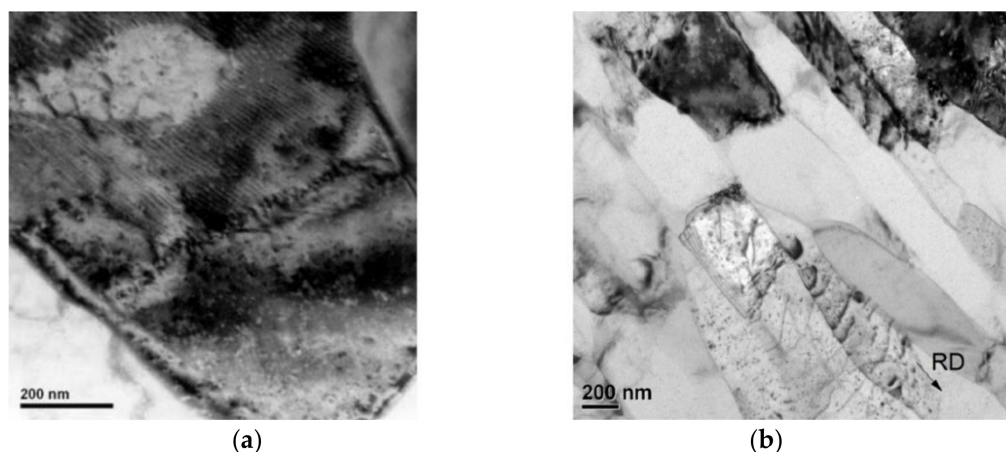


**Figure 38.** (a) TEM micrograph of pure Al after asymmetric cold rolling, reproduced from [149], with permission from Elsevier, 2009; (b) TEM micrograph of Al 1050 after asymmetric cryorolling [24] (RD—rolling direction).

In 2012, Yu et al. [24] reported about nanostructural Al 1050 sheets with a grain size of  $0.211 \mu\text{m}$  (Figure 38b). Sheets were manufactured using a novel method of asymmetric cryorolling. Asymmetric cryorolling ( $S_R = 1.4$ ) was performed by dipping the sheets into liquid nitrogen for at least 8 min before each rolling pass. The sheets were rolled with a total thickness reduction of 88.3% from 1.45 mm to 0.17 mm after seven rolling passes.

In 2009, Kim et al. [19] showed that ultrafine-grained Al-Mg-Si alloy (AA6061) sheets could be fabricated by SPD using high-ratio differential speed rolling (HRDSR) ( $S_R = 3$ ) and subsequent low-temperature aging. The asymmetric warm rolling was conducted on preheated specimens ( $120^\circ\text{C}$ ) and the work roll surfaces were maintained at  $140^\circ\text{C}$  throughout the process. Sheets with a width of 100 mm were rolled from 2 mm to 0.6 mm (70% thickness reduction) by a single pass. Processed sheets exhibited an ultra-high strength (yield stress: 455 MPa, ultimate tensile strength: 489 MPa, total elongation: 7.4%). The strengthening effect was impressive compared with the results obtained by using other SPD techniques. The high strength of the AA6061 could be attributed to a significant decrease in grain size ( $0.37 \mu\text{m}$ ) and increased Hall-Petch constant. The additional strengthening gained after the low-temperature aging was due to the precipitation of nanosized  $\beta'$  particles. Figure 39 shows the microstructures of the AA6061 observed by TEM [19].

In 2014, Loorentz and Y.G. Ko [134] reported about nanostructured AA5052 (with grains of  $0.7 \mu\text{m}$ ) manufactured by differential speed rolling ( $S_R = 4$ ). The sheets were rolled with a total thickness reduction of 75% from 4 mm to 1 mm after four rolling passes. The yield strength, ultimate tensile strength and total elongation of the initial sheets were  $65 \pm 5 \text{ MPa}$ ,  $137 \pm 10 \text{ MPa}$  and  $32 \pm 2\%$ , respectively. The yield strength and ultimate tensile strength of the nanostructured sheets were several times higher than that of the initial coarse counterpart:  $380 \pm 10 \text{ MPa}$  and  $390 \pm 10 \text{ MPa}$ , respectively. However, total elongation was decreased to  $4.2 \pm 0.5\%$  [134].

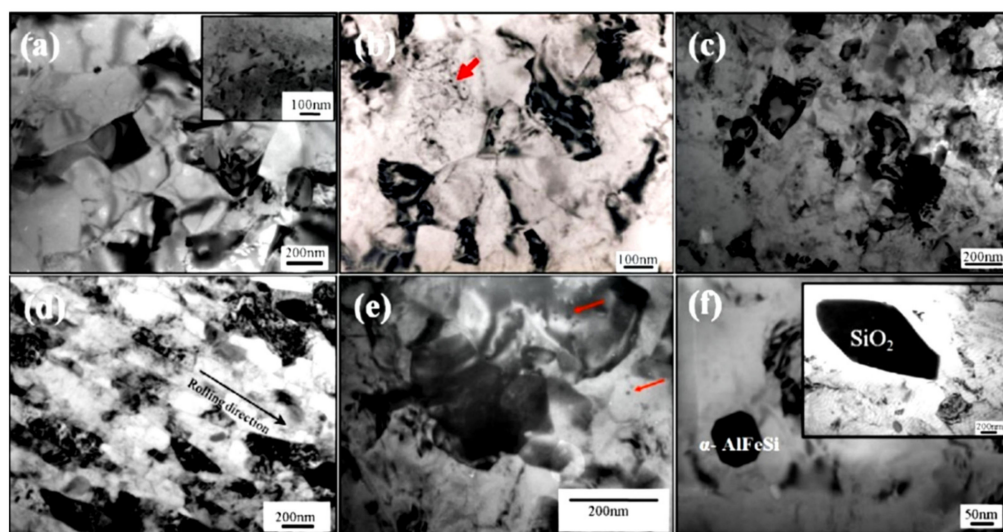


**Figure 39.** TEM micrographs of HRDSR AA6061 after thickness reduction of 70%: (a) furnace-cooled (FC) HRDSR Al, (b) water-quenched (WQ) HRDSR Al and (c) WQ-HRDSR Al after aging at 100 °C for 48 h. (d) WQ-HRDSR Al after aging at 100 °C for 48 h (taken on RD–ND plane) (e)  $\beta''$  or  $\beta'$  precipitates in the aged WQ-HRDSR Al (f)  $\text{SiO}_2$  (>200 nm) and  $\alpha\text{-AlFeSi}$  particles (~50 nm) commonly detected in all the HRDSR 6061 Al, reproduced from [19], with permission from Elsevier, 2009.

### 6. Asymmetric (Warm, Cold, Cryo) Rolling of Ti Alloys

Results of an extensive study (Tables 9–11 and Figure 40) showed that (warm, cold, cryo) differential speed rolling has a great impact on the grain size and mechanical properties of pure Ti and Ti-6Al-4V alloy. In 2010, Kim et al. [20] reported that high-strength CP-Ti (ASTM grade 2) sheets with ultrafine grains of 0.1–0.3  $\mu\text{m}$  and ultimate tensile strength of 895–915 MPa could be fabricated by single-pass high-ratio differential speed rolling (HRDSR) ( $S_R = 3$ ) at room temperature (thickness reduction of 63% from 2 mm to 0.74 mm).

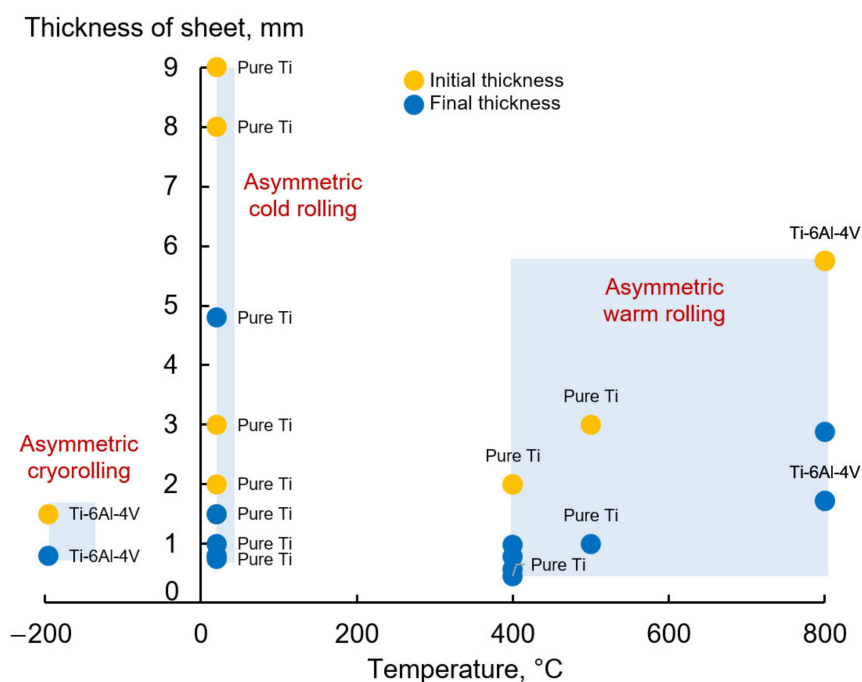


**Figure 40.** Different Ti alloys, which were processed by asymmetric (warm, cold, cryo) rolling (based on data from Tables 9–11).

**Table 9.** Experimental data related to asymmetric warm rolling of Ti alloys.

Material	Initial/Final Sheet Thickness, mm	Top/Bottom Work Roll Diameters, mm	Speed Ratio $S_R$	Total Reduction/Number of Passes	$T_r$ , °C	Final Grain Size, $\mu\text{m}$	Direction	YS, MPa	UTS, MPa	EL, %	Ref.
Pure Ti	2.0/1.18	300/300	1	41%/1	400	-	(0°)	451	507	25.1	[21]
							(45°)	437	476	26.9	
							(90°)	425	477	23.5	
	2.0/0.98	300/300	2	51%/1	400	-	(0°)	525	580	19.6	
							(45°)	456	511	23.1	
							(90°)	511	559	20.4	
	2.0/0.78	300/300	3	61%/1	400	-	(0°)	532	633	19.1	
							(45°)	507	550	20	
							(90°)	557	637	11.2	
	2.0/0.58	300/300	4	71%/1	400	-	(0°)	558	693	17.8	
							(45°)	502	562	15.3	
							(90°)	631	691	10.7	
	2.0/0.46	300/300	5	77%/1	400	-	(0°)	555	693	16.5	
							(45°)	494	550	17	
							(90°)	626	737	10.2	
Ti-6Al-4V	5.75/2.88	-	1.67	50%/-	800	0.227	-	1205	1273	18.7	[157]
	5.75/1.72	-	1.67	70%/-	800	0.229	-	1231	1365	22.8	
Pure Ti	3.0/1.0	-	1.36	66.7%/12	500	-	(0°)	232	385	35.4	[158]
							(45°)	247	356	44.7	
							(90°)	270	367	41	

**Table 10.** Experimental data related to asymmetric cold rolling of Ti alloys.

Material	Initial/Final Sheet Thickness, mm	Top/Bottom Work Roll Diameters, mm	Speed Ratio $S_R$	Total Reduction/Number of Passes	$T_r$ , °C	Final Grain Size, $\mu\text{m}$	Direction	YS, MPa	UTS, MPa	EL, %	Ref.
Pure Ti	9.0/1.5	130/130	1.5	83%/15	20	0.13	-	652	780	9.8	[159]
Pure Ti	3.0/1.0	-	1.36	66.7%/12	20	-	(0°)	236	397	39.8	[158]
							(45°)	278	372	42.4	
							(90°)	333	403	38.7	
Ti-6Al-4V	1.5/0.8	50/50	1.2	46.7%/-	20	-	-	-	1046	11.2	[160]
Pure Ti	2.0/0.74	400/400	3.0	63%/1	20	0.1-0.3	-	780	895	-	[20]
Pure Ti	8.0/4.8	180/180	1.5	40%/-	20	-	-	-	-	-	[161]

**Table 11.** Experimental data related to asymmetric cryorolling of Ti alloys.

Material	Initial/Final Sheet Thickness, mm	Top/Bottom Work Roll Diameters, mm	Speed Ratio $S_R$	Total Reduction/Number of Passes	$T_r$ , °C	Final Grain Size, $\mu\text{m}$	YS, MPa	UTS, MPa	EL, %	Ref.
Ti-6Al-4V	1.5/0.8	50/50	1.2	46.7%/-	-196	-	-	1113	10.1	[160]

The microstructure of the HRDSR-processed Ti was composed of two types of region: the “U” region, where shear bands were densely populated, and the “F” region, where some fragments of the original grains remained. The U region was clearly the dominant area fraction. The formation of nearly unidirectional shear bands is a characteristic of the HRDSR process, where large shear strain is imposed on the sheet. The interval of the lamellar boundaries in the U region was between 0.9 and 1.2  $\mu\text{m}$ . Very fine and equiaxed grains resided in shear bands and their sizes were comparable to or smaller than those of the lamellar spacing, indicating that the lamellar structure was related to the formation mechanism of ultrafine grains. Figure 41 shows TEM micrographs and the selected area electron diffraction (SAED) pattern of the HRDSR-processed Ti, taken at two places showing different microstructural features. There are two regions distinguished in the U region. One region (Figure 41a) is composed of elongated or nearly equiaxed subgrains with thick cell walls (0.2–0.3  $\mu\text{m}$  in size), inside of which the dislocation density is high. In the other region (Figure 41b), grains are more equiaxed and smaller. Comparison of the SAED pattern between the two regions indicates that the grains in the latter have higher angle grain boundaries. The SAED patterns in both regions can be indexed as the close-packed hexagonal structure of  $\alpha$ -Ti, indicating that no phase transformation occurred during rolling. The “A” region marked in Figure 41a indicates that the ultrafine grains were formed via a dynamic recovery process, by which the high density of dislocations forms equiaxed subgrains with low angle boundaries between the lamellar boundaries, which were then converted into equiaxed crystallites with high-angle boundaries via dynamic continuous recrystallization. As the local temperature in the shear bands can be greatly increased due to intense shear banding, dynamic recovery and recrystallization processes will be effectively promoted in the bands, even though the material is deformed at room temperature.

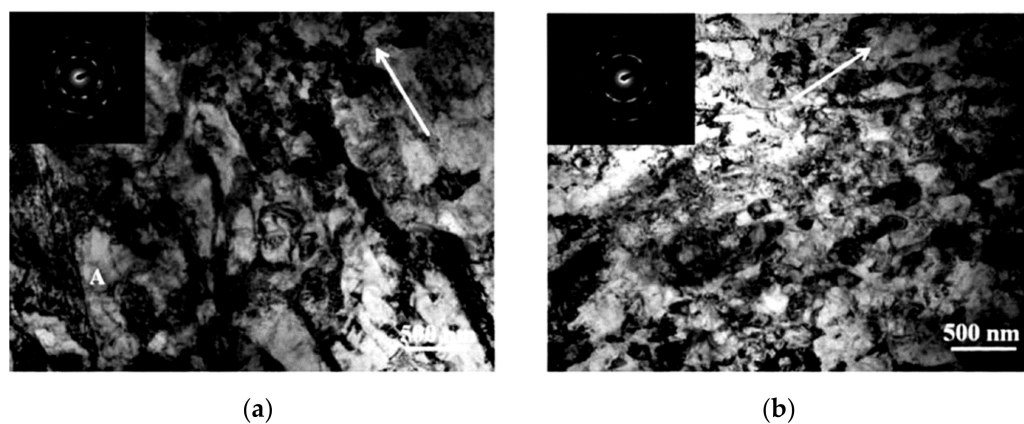


**Figure 41.** TEM micrographs and the selected area electron diffraction (SAED) pattern of the HRDSR-processed CP-Ti (ASTM grade 2). (a) Region with elongated or nearly equiaxed subgrains. (b) Region with equiaxed and smaller grains. The arrows indicate the rolling direction, reproduced from [20], with permission from Elsevier, 2010.

Extensive formation of high-density shear bands over the entire thickness of the section and their conversion to equiaxed crystallites with high-angle boundaries via dynamic recovery or dynamic continuous recrystallization were important in achieving ultrafine grains with a size of 0.1–0.3  $\mu\text{m}$  [20]. The resultant mechanical properties of pure Ti (Figure 42) exceeded those reported from tests using multiple passes of ECAP at elevated temperatures [162] or room temperature [163] and multiple cycles of accumulative roll bonding at room temperature [164].

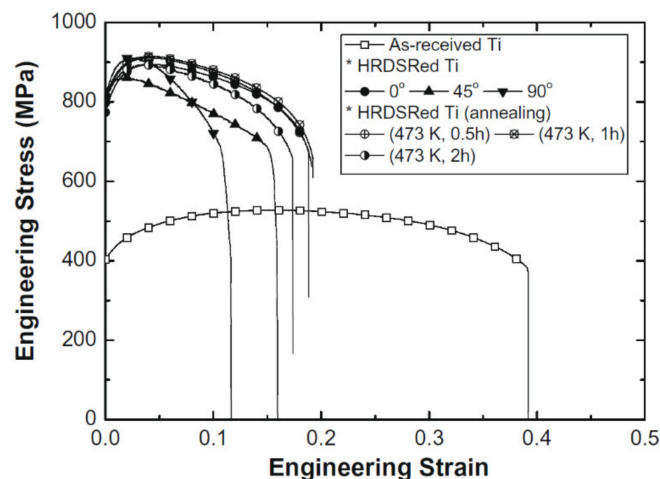


**Figure 42.** Stress–strain curves of the as-received and the HRDSR-processed Ti sheets, reproduced from [20], with permission from Elsevier, 2010.

A superior balance of strength (YS = 1231 MPa, UTS = 1365 MPa) and ductility (uniform elongation = 4.93%, total elongation = 22.8%) in Ti-6Al-4V alloy was achieved in 2016 by Chao et al. [157] through warm asymmetric rolling by a pair of rolls with different diameters with a ratio of 5:3 ( $S_R = 1.67$ ). The sheets were rolled with a total thickness reduction of 70% from 5.75 mm to 1.72 mm at 800 °C. The application of asymmetric rolling at 800 °C led to a higher strength–ductility balance, reaching the highest UTS  $\times$  TE of 30,000 MPa%. The exceptional mechanical properties were ascribed to the formation of an ultrafine-grained structure (0.229  $\mu\text{m}$ ), texture characteristics and transformation of the  $\beta$  phase upon straining.

## 7. Conclusions

Differential speed rolling, i.e., rolling with different angular speeds of the work rolls when both rolls are independently driven by two motors, is the most suitable way to implement asymmetric rolling in industry. A relatively low speed ratio of the work rolls ( $S_R \leq 1.5$ ) can be used for reducing rolling force, improving sheet flatness, minimizing the ski effect and obtaining thinner sheets. A high speed ratio of the work rolls ( $S_R = 2 \dots 4$ ) can be used as an SPD method for grain refinement and improvement of the texture and mechanical properties of large-scale sheets of Mg, Al and Ti pure metals and alloys.

The mechanics of the differential speed rolling process as an SPD method are based on simultaneous pure and simple shear, which combine the advantages of simple shear (rotation of the material as with ECAP) and the advantages of pure shear (compression and elongation of the material as with symmetric rolling). The mechanism for creating shear strain during differential speed rolling is the presence of the cross-shear zone in the deformation zone, in which the forces of contact friction are oppositely directed. The equivalent strain  $\bar{\epsilon} \geq 3 \dots 4$  can be obtained by single-pass differential speed rolling without lubrication (at high contact friction), when shear angle  $\varphi$  is no less than 80° due to the high speed ratio of the work rolls ( $S_R = 2 \dots 4$ ), large work roll diameter ( $D \geq 300$  mm), high thickness reduction per pass ( $\epsilon \geq 50\%$ ) and thinner initial thickness of the sheet ( $h_0 \leq 2$  mm).

Based on the analysis of publications related to asymmetric (hot, warm, cold, cryo) rolling, it was found that a superior balance of strength and ductility of Mg, Al and Ti alloys could be achieved:

- a. ultrafine-grained (0.6  $\mu\text{m}$ ) AZ31 sheets with YS of 382 MPa, UTS of 401 MPa and TE of 6.8% could be fabricated by differential speed rolling with high speed ratio of work rolls ( $S_R = 2$ ) at 150 °C followed by immediate water quenching;

- b. ultrafine-grained (0.37  $\mu\text{m}$ ) AA6061 sheets with YS of 455 MPa, UTS of 489 MPa, TE of 7.4% could be fabricated by differential speed rolling with high speed ratio of work rolls ( $S_R = 3$ ) at 120 . . . 140 °C and subsequent low temperature aging;
- c. ultrafine-grained (0.7  $\mu\text{m}$ ) AA5052 sheets with YS of 380 MPa, UTS of 390 MPa, TE of 4.2% could be fabricated by differential speed rolling with high speed ratio of work rolls ( $S_R = 4$ ) at room temperature;
- d. ultrafine-grained (0.1–0.3  $\mu\text{m}$ ) CP-Ti (ASTM grade 2) sheets with YS of 780 MPa, UTS of 895 MPa could be fabricated by differential speed rolling with high speed ratio of work rolls ( $S_R = 3$ ) at room temperature.

It should be noted, and it is very important, that the resulting mechanical properties of Mg, Al and Ti alloys are much better than those of conventionally cold-rolled materials and at least not worse than those of counterparts subjected to conventional SPD methods, such as ECAP, while having an undeniable advantage in terms of the possibility of the production of large-scale sheets. Future prospects for the development of differential speed rolling technologies lie in the optimization of process parameters, as well as in the industrial application of these technologies to a wider range of processed materials.

**Author Contributions:** Conceptualization, D.P.; formal analysis, A.P., P.T.; investigation, D.P.; writing—original draft preparation, D.P.; writing—review and editing, A.P., P.T.; supervision, A.P.; project administration, A.P.; funding acquisition, A.P. All authors have read and agreed to the published version of the manuscript.

**Funding:** The study was carried out within the framework of the implementation of the Resolution of the Government of the Russian Federation of 9 April 2010, No. 220 (Contract No. 075-15-2019-869 from 12 May 2019) and by a grant of the Russian Science Foundation (project No. 20-69-46042 of 20 May 2020).

**Institutional Review Board Statement:** Not applicable.

**Informed Consent Statement:** Not applicable.

**Data Availability Statement:** The data presented in this study are available on request from the corresponding author.

**Conflicts of Interest:** The authors declare no conflict of interest.

## References

1. Siebel, E. Zur Theorie des Walzvorganges bei ungleich angetriebenen Walzen. *Arch. Eisenhüttenwesen* **1941**, *15*, 125–128. [[CrossRef](#)]
2. Sachs, G.; Klinger, L.J. The Flow of Metals through Tools of Circular Contour. *J. Appl. Mech.* **1947**, *14*, 88–98. [[CrossRef](#)]
3. Razuvaev, D.S. A Method of Rolling Metal. USSR Patent 63448, 19 March 1940. (In Russian)
4. Chekmarev, A.P.; Nefedov, A.A. Rolling with unequal diameter rolls (complex cases of rolling). *Obrab. Met. Davl.* **1956**, *4*, 2–15. (In Russian)
5. Holbrook, R.L.; Zorowski, C.F. Effects of Nonsymmetry in Strip Rolling on Single-Roll Drive Mills. *J. Eng. Ind.* **1966**, *88*, 401–408. [[CrossRef](#)]
6. Johnson, W.; Needham, G. Further experiments in asymmetrical rolling. *Int. J. Mech. Sci.* **1966**, *8*, 443–455. [[CrossRef](#)]
7. Dewhurst, P.; Collins, I.F.; Johnson, W. A theoretical and experimental investigation into asymmetrical hot rolling. *Int. J. Mech. Sci.* **1974**, *16*, 389–397. [[CrossRef](#)]
8. Collins, I.F.; Dewhurst, P. A slipline field analysis of asymmetrical hot rolling. *Int. J. Mech. Sci.* **1975**, *17*, 643–651. [[CrossRef](#)]
9. Pan, D.; Sansome, D.H. An experimental study of the effect of roll-speed mismatch on the rolling load during the cold rolling of thin strip. *J. Mech. Work. Technol.* **1982**, *6*, 361–377. [[CrossRef](#)]
10. Dyja, H.; Korczak, P.; Pilarczyk, J.W.; Grzybowski, J. Theoretical and experimental analysis of plates asymmetric rolling. *J. Mater. Process. Technol.* **1994**, *45*, 167–172. [[CrossRef](#)]
11. Dyja, H.; Markowski, J.; Stoiniski, D. Asymmetry of the roll gap as a factor improving work of the hydraulic gauge control in the plate rolling mill. *J. Mater. Process. Technol.* **1996**, *60*, 73–80. [[CrossRef](#)]
12. Richelsen, A.B. Elastic-plastic analysis of the stress and strain distributions in asymmetric rolling. *Int. J. Mech. Sci.* **1997**, *39*, 1199–1211. [[CrossRef](#)]
13. Salganik, V.M.; Pesin, A.M. *Asimmetrichnaya Tonkolistovaya Prokatka: Razvitiye Teorii, Tekhnologii i Novyye Resheniya [Asymmetric Sheet Rolling: Development of Theory, Technology and New Solutions]*; MISIS Publisher: Moscow, Russia, 1997; p. 192. (In Russian)

14. Choi, C.-H.; Kim, K.-H.; Lee, D.N. The effect of shear texture development on the formability in rolled aluminum alloy sheets. *Mater. Sci. Forum* **1998**, *273–275*, 391–396. [[CrossRef](#)]
15. Cui, Q.; Ohori, K. Grain refinement of high purity aluminium by asymmetric rolling. *Mater. Sci. Technol.* **2000**, *16*, 1095–1101. [[CrossRef](#)]
16. Kim, W.J.; Lee, J.B.; Kim, W.Y.; Jeong, H.T.; Jeong, H.G. Microstructure and mechanical properties of Mg-Al-Zn alloy sheets severely deformed by asymmetrical rolling. *Scr. Mater.* **2007**, *56*, 309–312. [[CrossRef](#)]
17. Ji, Y.H.; Park, J.J.; Kim, W.J. Finite element analysis of severe deformation in Mg-3Al-1Zn sheets through differential-speed rolling with a high-speed ratio. *Mater. Sci. Eng. A* **2007**, *454–455*, 570–574. [[CrossRef](#)]
18. Kim, W.J.; Kim, M.J.; Wang, J.Y. Superplastic behavior of a fine-grained ZK60 magnesium alloy processed by high-ratio differential speed rolling. *Mater. Sci. Eng. A* **2009**, *527*, 322–327. [[CrossRef](#)]
19. Kim, W.J.; Wang, J.Y.; Choi, S.O.; Choi, H.J.; Sohn, H.T. Synthesis of ultra high strength Al-Mg-Si alloy sheets by differential speed rolling. *Mater. Sci. Eng. A* **2009**, *520*, 23–28. [[CrossRef](#)]
20. Kim, W.J.; Yoo, S.J.; Lee, J.B. Microstructure and mechanical properties of pure Ti processed by high-ratio differential speed rolling at room temperature. *Scr. Mater.* **2010**, *62*, 451–454. [[CrossRef](#)]
21. Kim, W.J.; Yoo, S.J.; Jeong, H.T.; Kim, D.M.; Choe, B.H.; Lee, J.B. Effect of the speed ratio on grain refinement and texture development in pure Ti during differential speed rolling. *Scr. Mater.* **2011**, *64*, 49–52. [[CrossRef](#)]
22. Loorentz; Ko, Y.G. Microstructure evolution and mechanical properties of severely deformed Al alloy processed by differential speed rolling. *J. Alloy. Compd.* **2012**, *536*, S122–S125. [[CrossRef](#)]
23. Polkowski, W.; Jozwik, P.; Polanski, M.; Bojar, Z. Microstructure and texture evolution of copper processed by differential speed rolling with various speed asymmetry coefficient. *Mater. Sci. Eng. A* **2013**, *564*, 289–297. [[CrossRef](#)]
24. Yu, H.L.; Lu, C.; Tieu, K.; Liu, X.H.; Sun, Y.; Yu, Q.B.; Kong, C. Asymmetric cryorolling for fabrication of nanostructural aluminum sheets. *Sci. Rep.* **2012**, *2*, 772. [[CrossRef](#)] [[PubMed](#)]
25. Yu, H.L.; Tieu, K.; Lu, C.; Liu, X.H.; Godbole, A.; Kong, C. Mechanical properties of Al-Mg-Si alloy sheets produced using asymmetric cryorolling and ageing treatment. *Mater. Sci. Eng. A* **2013**, *568*, 212–218. [[CrossRef](#)]
26. Yu, H.L.; Tieu, K.; Lu, C.; Lou, Y.S.; Liu, X.H.; Godbole, A.; Kong, C. Tensile fracture of ultrafine grained aluminum 6061 sheets by asymmetric cryorolling for microforming. *Int. J. Damage Mech.* **2014**, *23*, 1077–1095. [[CrossRef](#)]
27. Vincze, G.; Simoes, F.J.P.; Butuc, M.C. Asymmetrical Rolling of Aluminum Alloys and Steels: A Review. *Metals* **2020**, *10*, 1126. [[CrossRef](#)]
28. Kraner, J.; Smolar, T.; Volsak, D.; Cvahte, P.; Godec, M.; Paulin, I. A review of asymmetric rolling. *Mater. Technol.* **2020**, *54*, 731–743. [[CrossRef](#)]
29. Philipp, M.; Schwenzfeier, W.; Fischer, F.D.; Wodlinger, R.; Fischer, C. Front end bending in plate rolling influenced by circumferential speed mismatch and geometry. *J. Mater. Process. Technol.* **2007**, *184*, 224–232. [[CrossRef](#)]
30. Anders, D.; Münker, T.; Artel, J.; Weinberg, K. A dimensional analysis of front-end bending in plate rolling applications. *J. Mater. Process. Technol.* **2012**, *212*, 1387–1398. [[CrossRef](#)]
31. Balgabekov, T.K.; Azbanbayev, E.M.; Isagulov, A.Z.; Isagulova, D.A.; Zakariya, N.B.; Yermaganbetov, N.Z.; Kenzhekeeva, A.R.; Konirova, Z.A. Effect of Asymmetric Rolling with Cone-Shaped Rolls on Microstructure and Tensile Properties of Low-Carbon Steel. *Adv. Mater. Res.* **2015**, *1105*, 149–153. [[CrossRef](#)]
32. Azbanbayev, E.M. Research and development of production technology of metals with nanostructure and high mechanical properties during the rolling in the back-taper rolls. Ph.D. Thesis, Karaganda State Technical University, Karaganda, Kazakhstan, December 2015. (In Russian)
33. Hartung, H.G.; Klamma, K.; Rohde, W.; Seidel, J. Roll Stand Comprising a Crown-Variable-Control (CVC) Roll Pair. US Patent 7,059,163, 13 June 2006.
34. Kiyoshi, N.; Hori, Y.; Ogawa, S.; Mizutani, Y.; Kojima, A. High reduction rolling technology on pair cross mill. *Nippon. Steel Technol. Rep.* **1997**, *75*, 9–23.
35. Wronski, S.; Wierzbanski, K.; Wronski, M.; Bacroix, B. Three-dimensional analysis of asymmetric rolling with flat and inclined entry. *Arch. Metall. Mater.* **2014**, *59*, 585–591. [[CrossRef](#)]
36. Gao, H.; Ramalingam, S.C.; Barber, G.C.; Chen, G. Analysis of asymmetrical cold rolling with varying coefficients of friction. *J. Mater. Process. Technol.* **2002**, *124*, 178–182. [[CrossRef](#)]
37. Utsunomiya, H.; Ueno, T.; Sakai, T. Improvement in the r-value of aluminum sheets by differential-friction rolling. *Scr. Mater.* **2007**, *57*, 1109–1112. [[CrossRef](#)]
38. Kasai, D.; Komori, A.; Ishii, A.; Yamada, K.; Ogawa, S. Strip Warp Behavior and Mechanism in Single Roll Driven Rolling. *ISIJ Int.* **2016**, *56*, 1815–1824. [[CrossRef](#)]
39. Sakai, T.; Hamada, S.; Saito, Y. Improvement of the r-value in 5052 aluminum alloy sheets having through-thickness shear texture by 2-pass single-roll drive unidirectional shear rolling. *Scr. Mater.* **2001**, *44*, 2569–2573. [[CrossRef](#)]
40. Pesin, A. Modeling and Development of Asymmetric Deformation Processes to Improve the Efficiency of Sheet Rolling. Ph.D. Thesis, Nosov Magnitogorsk State Technical University, Magnitogorsk, Russia, 2003. (In Russian)
41. Potapkin, V.F.; Fedorinov, V.A.; Morozov, I.A.; Ravich, A.S. Klet' Dlya Deformatsii Metalla Mezhdru Nepodvizhnym i Rabochim Privodnymi Valkami [Stand for Metal Deformation Between Stationary and Driven Work Rolls]. USSR Patent 871855, 30 September 1979. (In Russian)

42. Pesin, A. Regularities of Asymmetric Deformation and Increasing the Efficiency of the Cold Sheet Rolling Process. Ph.D. Thesis, Nosov Magnitogorsk State Technical University, Magnitogorsk, Russia, 1989. (In Russian)
43. Vydrin, V.N. *Dinamika Prokatnykh Stanov [The Dynamics of Rolling Mills]*; Metallurgizdat Publisher: Sverdlovsk, Russia, 1960; p. 255. (In Russian)
44. Vydrin, V.N.; Ageyev, L.M. Printsipial'nyye i teoreticheskiye osnovy novogo protsessa "prokatka-volocheniye" [Fundamental and theoretical foundations of the new process "rolling-drawing"]. *Teoriya i tekhnologiya prokatki Chelyabinsk* **1971**, *76*, 3–21. (In Russian)
45. Shimoyama, K.; Yokoyama, S.; Kaneko, S.; Fujita, F. Effect of grooved roll profiles on microstructure evolutions of AZ31 sheets in Periodical Straining Rolling process. *Mater. Sci. Eng. A* **2014**, *611*, 58–68. [[CrossRef](#)]
46. Li, L.; Nagai, K.; Yin, F.X. Progress in Cold Roll Bonding of Metals. *Sci. Technol. Adv. Mater.* **2008**, *9*, 1–11. [[CrossRef](#)]
47. Li, X.; Zu, G.; Ding, M.; Mu, Y.; Wang, P. Interfacial microstructure and mechanical properties of Cu/Al clad sheet fabricated by asymmetrical roll bonding and annealing. *Mater. Sci. Eng. A* **2011**, *529*, 485–491. [[CrossRef](#)]
48. Wang, T.; Wang, Y.; Bian, L.; Huang, Q. Microstructural evolution and mechanical behavior of Mg/Al laminated composite sheet by novel corrugated rolling and flat rolling. *Mater. Sci. Eng. A* **2019**, *765*, 138318. [[CrossRef](#)]
49. Wang, T.; Li, S.; Ren, Z.; Jia, Y.; Fu, W.; Guo, M.; Ma, X.; Han, J. Microstructure Characterization and Mechanical Property of Mg/Al Laminated Composite Prepared by the Novel Approach: Corrugated + Flat Rolling (CFR). *Metals* **2019**, *9*, 690. [[CrossRef](#)]
50. Wang, T.; Liu, W.; Liu, Y.; Wang, Z.; Ignatov, A.V.; Huang, Q. Formation mechanism of dynamic multi-neutral points and cross shear zones in corrugated rolling of Cu/Al laminated composite. *J. Mater. Process. Technol.* **2021**, *295*, 117157. [[CrossRef](#)]
51. Pesin, A.; Pustovoitov, D.; Biryukova, O.; Ilyina, N. FEM simulation of fabrication of Al-steel layered composites with mechanical bonding through the interfacial concavo-convex lock effect. *Procedia Manuf.* **2020**, *50*, 579–583. [[CrossRef](#)]
52. Hirt, G.; Thome, M. Rolling of functional metallic surface structures. *CIRP Ann.* **2008**, *57*, 317–320. [[CrossRef](#)]
53. Hirt, G.; Thome, M. Large area rolling of functional metallic micro structures. *Prod. Eng. Res. Devel.* **2007**, *1*, 351–356. [[CrossRef](#)]
54. Stille, S.; Beck, T.; Singheiser, L. Influence of riblet geometry on fatigue life of surface structured AA 2024 thin sheets. *Int. J. Fatigue* **2014**, *68*, 48–55. [[CrossRef](#)]
55. Zuo, Y.; Fu, X.; Cui, J.; Tang, X.; Mao, L.; Li, L.; Zhu, Q. Shear deformation and plate shape control of hot-rolled aluminium alloy thick plate prepared by asymmetric rolling process. *Trans. Nonferrous Met. Soc. China* **2014**, *24*, 2220–2225. [[CrossRef](#)]
56. Tian, Y.; Guo, Y.C.; Wang, Z.-D.; Wang, G.-D. Analysis of rolling pressure in asymmetrical rolling process by slab method. *J. Iron Steel Res. Int.* **2009**, *16*, 22–26. [[CrossRef](#)]
57. Park, J.-J. Finite-element analysis of severe plastic deformation in differential-speed rolling. *Comput. Mater. Sci.* **2015**, *100*, 61–66. [[CrossRef](#)]
58. Pesin, A.M.; Pustovoytov, D.O.; Shveeva, T.V.; Steblyanko, V.L.; Fedoseev, S.A. Simulation of nonmonotonic metal flow during asymmetric sheet rolling with different velocities of the rolls. *Vestn. Nosov Magnitogorsk. State Tech. Univ.* **2017**, *15*, 56–63. [[CrossRef](#)]
59. Zuo, F.; Jiang, J.; Shan, A.; Fang, J.; Zhang, X. Shear deformation and grain refinement in pure Al by asymmetric rolling. *Trans. Nonferrous Met. Soc. China* **2008**, *18*, 774–777. [[CrossRef](#)]
60. Sidor, J.; Miroux, A.; Petrov, R.; Kestens, L. Microstructural and crystallographic aspects of conventional and asymmetric rolling processes. *Acta Mater.* **2008**, *56*, 2495–2507. [[CrossRef](#)]
61. Pesin, A.; Pustovoytov, D. Influence of process parameters on distribution of shear strain through sheet thickness in asymmetric rolling. *Key Eng. Mater.* **2014**, *622*, 929–935. [[CrossRef](#)]
62. Polkowski, W. *Differential Speed Rolling: A New Method for a Fabrication of Metallic Sheets with Enhanced Mechanical Properties, Progress in Metallic Alloys, Vadim Glebovsky*; IntechOpen: London, UK, 2016. Available online: <https://www.intechopen.com/books/progress-in-metallic-alloys/differential-speed-rolling-a-new-method-for-a-fabrication-of-metallic-sheets-with-enhanced-mechanica> (accessed on 20 April 2021). [[CrossRef](#)]
63. Shrivastava, S.; Ghosh, C.; Jonas, J.J. A comparison of the von Mises and Hencky equivalent strains for use in simple shear experiments. *Philos. Mag.* **2012**, *92*, 779–786. [[CrossRef](#)]
64. Shrivastava, S.C.; Jonas, J.J.; Canova, G. Equivalent strain in large deformation torsion testing: Theoretical and practical considerations. *J. Mech. Phys. Solids* **1982**, *30*, 75–90. [[CrossRef](#)]
65. Onaka, S. Equivalent strain in simple shear deformation described by using the Hencky strain. *Philos. Mag. Lett.* **2010**, *90*, 633–639. [[CrossRef](#)]
66. Polakowski, N.H.; Ripling, E.J. *Strength and Structure of Engineering Materials*; Prentice-Hall: Hoboken, NJ, USA, 1966; pp. 381–383.
67. Beygelzimer, Y. Equivalent strain in simple shear of metals. *Phys. Technol. High Press.* **2015**, *25*, 90–97.
68. Saito, Y.; Sakai, T.; Maeda, F.; Kato, K. Deformation and recrystallization behavior of ferritic stainless steel in high speed hot rolling. *Tetsu Hagane (ISIJ)* **1986**, *72*, 799–806. [[CrossRef](#)]
69. Sakai, T.; Saito, Y.; Hirano, K.; Kato, K. Deformation and recrystallization behavior of low carbon steel in high speed hot rolling. *Trans. ISIJ* **1988**, *28*, 1028–1035. [[CrossRef](#)]
70. Angella, G.; Esfandiari Jahromi, B.; Vedani, M. A comparison between equal channel angular pressing and asymmetric rolling of silver in the severe plastic deformation regime. *Mater. Sci. Eng. A* **2013**, *559*, 742–750. [[CrossRef](#)]
71. Kang, S.-B.; Min, B.-K.; Kim, H.-W.; Wilkinson, D.S.; Kang, J. Effect of asymmetric rolling on the texture and mechanical properties of AA6111-aluminum sheet. *Metall. Mater. Trans. A* **2005**, *36*, 3141–3149. [[CrossRef](#)]

72. Ma, C.; Hou, L.; Zhang, J.; Zhuang, L. Influence of thickness reduction per pass on strain, microstructures and mechanical properties of 7050 Al alloy sheet processed by asymmetric rolling. *Mater. Sci. Eng. A* **2016**, *650*, 454–468. [CrossRef]
73. Pesin, A.; Pustovoytov, D.; Shveyova, T.; Vafin, R. Finite element simulation and comparison of a shear strain and equivalent strain during ECAP and asymmetric rolling. *IOP Conf. Ser. Mater. Sci. Eng.* **2017**, *293*, 012007. [CrossRef]
74. Megantoro, R.B.; Loorentz; Ko, Y.G. Temperature rise during differential speed rolling. *J. Alloy. Compd.* **2014**, *586*, S254–S257. [CrossRef]
75. Pesin, A.M.; Pustovoytov, D.O.; Vafin, R.K. Simulation of temperature fields in a deformation zone during asymmetric rolling of aluminum alloys. *Vestn. Nosov Magnitogorsk. State Tech. Univ.* **2015**, *4*, 75–81.
76. Pesin, A.; Pustovoytov, D. Heat transfer modeling in asymmetrical sheet rolling of aluminium alloys with ultra high shear strain. *MATEC Web Conf.* **2016**, *80*, 04005. [CrossRef]
77. Simões, F.J.P. Asymmetrical rolling of an aluminum alloy 1050. Ph.D. Thesis, Universidade de Aveiro, Aveiro, Portugal, 2008; p. 152. Available online: <http://hdl.handle.net/10773/2560> (accessed on 20 April 2021).
78. Lee, S.H.; Lee, D.N. Analysis of deformation textures of asymmetrically rolled steel sheets. *Int. J. Mech. Sci.* **2001**, *43*, 1997–2015. [CrossRef]
79. Lee, J.K.; Lee, D.N. Texture control and grain refinement of AA1050 Al alloy sheets by asymmetric rolling. *Int. J. Mech. Sci.* **2008**, *50*, 869–887. [CrossRef]
80. Bobor, K.; Hegedus, Z.; Gubicza, J.; Barkai, I.; Pekker, P.; Krallics, G. Microstructure and mechanical properties of Al 7075 alloy processed by differential speed rolling. *Period. Polytech. Mech. Eng.* **2012**, *56*, 111–115. [CrossRef]
81. Pesin, A.; Pustovoytov, D. Finite Element Simulation of Shear Strain during High-Ratio Differential Speed Rolling of Aluminum Alloy 5083. *Key Eng. Mater.* **2016**, *716*, 700–707. [CrossRef]
82. Kim, K.-H.; Lee, D.N. Analysis of deformation textures of asymmetrically rolled aluminum sheets. *Acta Mater.* **2001**, *49*, 2583–2595. [CrossRef]
83. Lee, D.N. Asymmetric Rolling as Means of Texture and Ridging Control and Grain Refinement of Aluminum Alloy and Steel Sheets. *Mater. Sci. Forum* **2004**, *449–452*, 1–6. [CrossRef]
84. Hamad, K.; Ko, Y.G. A cross-shear deformation for optimizing the strength and ductility of AZ31 magnesium alloys. *Sci. Rep.* **2016**, *6*, 29954. [CrossRef] [PubMed]
85. Ko, Y.G.; Hamad, K. Structural features and mechanical properties of AZ31 Mg alloy warm-deformed by differential speed rolling. *J. Alloy. Compd.* **2018**, *744*, 96–103. [CrossRef]
86. Lee, J.K.; Lee, D.N. Shear Texture Development and Grain Refinement in Asymmetrically Rolled Aluminum Alloy Sheets by Varied Reduction per Pass. *Mater. Sci. Forum* **2002**, *408–412*, 1419–1424. [CrossRef]
87. Beausir, B.; Biswas, S.; Kim, D.; Toth, L.S.; Suwas, S. Analysis of microstructure and texture evolution in pure magnesium during symmetric and asymmetric rolling. *Acta Mater.* **2009**, *57*, 5061–5077. [CrossRef]
88. Biswas, S.; Kim, D.; Suwas, S. Asymmetric and symmetric rolling of magnesium: Evolution of microstructure, texture and mechanical properties. *Mater. Sci. Eng. A* **2012**, *550*, 19–30. [CrossRef]
89. Seong, J.W.; Kim, W.J. Development of biodegradable Mg-Ca alloy sheets with enhanced strength and corrosion properties through the refinement and uniform dispersion of the Mg<sub>2</sub>Ca phase by high-ratio differential speed rolling. *Acta Biomater.* **2015**, *11*, 531–542. [CrossRef]
90. Gong, X.; Kang, S.B.; Cho, J.H.; Li, S. Effect of annealing on microstructure and mechanical properties of ZK60 magnesium alloy sheets processed by twin-roll cast and differential speed rolling. *Mater. Charact.* **2014**, *97*, 183–188. [CrossRef]
91. Ucuncuoglu, S.; Ekerim, A.; Secgin, G.O.; Duygulu, O. Effect of asymmetric rolling process on the microstructure, mechanical properties and texture of AZ31 magnesium alloys sheets produced by twin roll casting technique. *J. Magnes. Alloy.* **2014**, *2*, 92–98. [CrossRef]
92. Kaseem, M.; Chung, B.K.; Yang, H.W.; Hamad, K.; Ko, Y.G. Effect of Deformation Temperature on Microstructure and Mechanical Properties of AZ31 Mg Alloy Processed by Differential-Speed Rolling. *J. Mater. Sci. Technol.* **2015**, *31*, 498–503. [CrossRef]
93. Luo, D.; Wang, H.-Y.; Zhao, L.-G.; Wang, C.; Liu, G.-J.; Liu, Y.; Jiang, Q.-C. Effect of differential speed rolling on the room and elevated temperature tensile properties of rolled AZ31 Mg alloy sheets. *Mater. Charact.* **2017**, *124*, 223–228. [CrossRef]
94. Watanabe, H.; Mukai, T.; Ishikawa, K. Effect of temperature of differential speed rolling on room temperature mechanical properties and texture in an AZ31 magnesium alloy. *J. Mater. Process. Technol.* **2007**, *182*, 644–647. [CrossRef]
95. Tolouie, E.; Jamaati, R. Effect of  $\beta$ -Mg<sub>17</sub>Al<sub>12</sub> phase on microstructure, texture and mechanical properties of AZ91 alloy processed by asymmetric hot rolling. *Mater. Sci. Eng. A* **2018**, *738*, 81–89. [CrossRef]
96. Huang, X.; Suzuki, K.; Watazu, A.; Shigematsu, I.; Saito, N. Effects of thickness reduction per pass on microstructure and texture of Mg–3Al–1Zn alloy sheet processed by differential speed rolling. *Scr. Mater.* **2009**, *60*, 964–967. [CrossRef]
97. Gong, X.; Kang, S.B.; Li, S.; Cho, J.H. Enhanced plasticity of twin-roll cast ZK60 magnesium alloy through differential speed rolling. *Mater. Des.* **2009**, *30*, 3345–3350. [CrossRef]
98. Huang, X.; Suzuki, K.; Watazu, A.; Shigematsu, I.; Saito, N. Improvement of formability of Mg–Al–Zn alloy sheet at low temperatures using differential speed rolling. *J. Alloy. Compd.* **2009**, *470*, 263–268. [CrossRef]
99. Huang, X.; Suzuki, K.; Watazu, A.; Shigematsu, I.; Saito, N. Mechanical properties of Mg–Al–Zn alloy with a tilted basal texture obtained by differential speed rolling. *Mater. Sci. Eng. A* **2008**, *488*, 214–220. [CrossRef]

100. Huang, X.; Suzuki, K.; Watazu, A.; Shigematsu, I.; Saito, N. Microstructural and textural evolution of AZ31 magnesium alloy during differential speed rolling. *J. Alloys Compd.* **2009**, *479*, 726–731. [[CrossRef](#)]
101. Chang, L.L.; Cho, J.H.; Kang, S.B. Microstructure and mechanical properties of AM31 magnesium alloys processed by differential speed rolling. *J. Mater. Process. Technol.* **2011**, *211*, 1527–1533. [[CrossRef](#)]
102. Xia, W.; Chen, Z.; Chen, D.; Zhu, S. Microstructure and mechanical properties of AZ31 magnesium alloy sheets produced by differential speed rolling. *J. Mater. Process. Technol.* **2009**, *209*, 26–31. [[CrossRef](#)]
103. Huang, X.; Suzuki, K.; Saito, N. Microstructure and mechanical properties of AZ80 magnesium alloy sheet processed by differential speed rolling. *Mater. Sci. Eng. A* **2009**, *508*, 226–233. [[CrossRef](#)]
104. Chang, L.L.; Cho, J.H.; Kang, S.K. Microstructure and mechanical properties of twin roll cast AM31 magnesium alloy sheet processed by differential speed rolling. *Mater. Des.* **2012**, *34*, 746–752. [[CrossRef](#)]
105. Kim, Y.S.; Kim, W.J. Microstructure and superplasticity of the as-cast Mg-9Al-1Zn magnesium alloy after high-ratio differential speed rolling. *Mater. Sci. Eng. A* **2016**, *677*, 332–339. [[CrossRef](#)]
106. Huang, X.; Suzuki, K.; Watazu, A.; Shigematsu, I.; Saito, N. Microstructure and texture of Mg-Al-Zn alloy processed by differential speed rolling. *J. Alloy. Compd.* **2008**, *457*, 408–412. [[CrossRef](#)]
107. Kwak, T.Y.; Lim, H.K.; Han, S.H.; Kim, W.J. Refinement of the icosahedral quasicrystalline phase and the grain size of Mg-9.25Zn-1.66Y alloy by high-ratio differential speed rolling. *Scr. Mater.* **2015**, *103*, 49–52. [[CrossRef](#)]
108. Huang, X.; Suzuki, K.; Chino, Y. Static recrystallization and mechanical properties of Mg-4Y-3RE magnesium alloy sheet processed by differential speed rolling at 823 K. *Mater. Sci. Eng. A* **2012**, *538*, 281–287. [[CrossRef](#)]
109. Kwak, T.Y.; Kim, W.J. Superplastic behavior of an ultrafine-grained Mg-13Zn-1.55Y alloy with a high volume fraction of icosahedral phases prepared by high-ratio differential speed rolling. *J. Mater. Sci. Technol.* **2017**, *33*, 919–925. [[CrossRef](#)]
110. Kim, S.-H.; You, B.-S.; Yim, C.D.; Seo, Y.-M. Texture and microstructure changes in asymmetrically hot rolled AZ31 magnesium alloy sheets. *Mater. Lett.* **2005**, *59*, 3876–3880. [[CrossRef](#)]
111. Ji, Y.H.; Park, J.J. Analysis of thermo-mechanical process occurred in magnesium alloy AZ31 sheet during differential speed rolling. *Mater. Sci. Eng. A* **2008**, *485*, 299–304. [[CrossRef](#)]
112. Cho, J.-H.; Kim, H.-W.; Kang, S.-B.; Han, T.-S. Bending behavior, and evolution of texture and microstructure during differential speed warm rolling of AZ31B magnesium alloys. *Acta Mater.* **2011**, *59*, 5638–5651. [[CrossRef](#)]
113. Li, X.; Li, X.; Ye, Y.; Zhang, R.; Kure-Chu, S.-Z.; Tang, G. Deformation mechanisms and recrystallization behavior of Mg-3Al-1Zn and Mg-1Gd alloys deformed by electroplastic-asymmetric rolling. *Mater. Sci. Eng. A* **2019**, *742*, 722–733. [[CrossRef](#)]
114. Lee, J.B.; Konno, T.J.; Jeong, H.G. Effect of differential speed rolling on the anisotropy of mechanical properties and texture evolution of AZ31 Mg alloys. *J. Alloy. Compd.* **2010**, *499*, 273–277. [[CrossRef](#)]
115. Kim, W.J.; Hwang, B.G.; Lee, M.J.; Park, Y.B. Effect of speed-ratio on microstructure, and mechanical properties of Mg-3Al-1Zn alloy, in differential speed rolling. *J. Alloy. Compd.* **2011**, *509*, 8510–8517. [[CrossRef](#)]
116. Kim, W.J.; Lee, Y.G.; Lee, M.J.; Wang, J.Y.; Park, Y.B. Exceptionally high strength in Mg-3Al-1Zn alloy processed by high-ratio differential speed rolling. *Scr. Mater.* **2011**, *65*, 1105–1108. [[CrossRef](#)]
117. Kim, W.Y.; Kim, W.J. Fabrication of ultrafine-grained Mg-3Al-1Zn magnesium alloy sheets using a continuous high-ratio differential speed rolling technique. *Mater. Sci. Eng. A* **2014**, *594*, 189–192. [[CrossRef](#)]
118. Lee, J.B.; Konno, T.J.; Jeong, H.G. Grain refinement and texture evolution in AZ31 Mg alloys sheet processed by differential speed rolling. *Mater. Sci. Eng. B* **2009**, *161*, 166–169. [[CrossRef](#)]
119. Hamad, K.; Chung, B.K.; Ko, Y.G. Microstructure and mechanical properties of severely deformed Mg-3%Al-1%Zn alloy via isothermal differential speed rolling at 453 K. *J. Alloy. Compd.* **2014**, *615*, S590–S594. [[CrossRef](#)]
120. Kim, W.J.; Park, J.D.; Wang, J.Y.; Yoon, W.S. Realization of low-temperature superplasticity in Mg-Al-Zn alloy sheets processed by differential speed rolling. *Scr. Mater.* **2007**, *57*, 755–758. [[CrossRef](#)]
121. Tolouie, E.; Jamaati, R. Asymmetric cold rolling: A technique for achieving non-basal textures in AZ91 alloy. *Mater. Lett.* **2019**, *249*, 143–146. [[CrossRef](#)]
122. Kim, W.J.; Lee, B.H.; Lee, J.B.; Lee, M.J.; Park, Y.B. Synthesis of high-strain-rate superplastic magnesium alloy sheets using a high-ratio differential speed rolling technique. *Scr. Mater.* **2010**, *63*, 772–775. [[CrossRef](#)]
123. Lequeu, P.H.; Jonas, J.J. Modeling of the plastic anisotropy of textured sheet. *Metall. Mater. Trans.* **1988**, *19*, 105–120. [[CrossRef](#)]
124. Engler, O.; Kim, H.C.; Huh, M.Y. Formation of {111} fibre texture in recrystallized aluminium sheet. *Mater. Sci. Technol.* **2001**, *17*, 75–86. [[CrossRef](#)]
125. Jin, H.; Lloyd, D.J. The reduction of planar anisotropy by texture modification through asymmetric rolling and annealing in AA5754. *Mater. Sci. Eng. A* **2005**, *399*, 358–367. [[CrossRef](#)]
126. Ma, C.; Hou, L.; Zhang, J.; Zhuang, L. Effect of deformation routes on the microstructures and mechanical properties of the asymmetrical rolled 7050 Aluminum alloy plates. *Mater. Sci. Eng. A* **2018**, *733*, 307–315. [[CrossRef](#)]
127. Wronski, S.; Ghiliani, B.; Chauveau, T.; Bacroix, B. Analysis of textures heterogeneity in cold and warm asymmetrically rolled aluminium. *Mater. Charact.* **2011**, *62*, 22–34. [[CrossRef](#)]
128. Kim, H.-K.; Kim, H.-W.; Cho, J.-H.; Lee, J.-C. High-formability Al alloy sheet produced by asymmetric rolling of strip-cast sheet. *Mater. Sci. Eng. A* **2013**, *574*, 31–36. [[CrossRef](#)]
129. Cheon, B.-H.; Kim, H.-W.; Lee, J.-C. Asymmetric rolling of strip-cast Al-5.5Mg-0.3Cu alloy sheet: Effects on the formability and mechanical properties. *Mater. Sci. Eng. A* **2011**, *528*, 5223–5227. [[CrossRef](#)]

130. Li, S.; Qin, N.; Liu, J.; Zhang, X. Microstructure, texture and mechanical properties of AA1060 aluminum plate processed by snake rolling. *Mater. Des.* **2016**, *90*, 1010–1017. [[CrossRef](#)]
131. Goli, F.; Jamaati, R. Asymmetric cross rolling (ACR): A novel technique for enhancement of Goss/Brass texture ratio in Al-Cu-Mg alloy. *Mater. Charact.* **2018**, *142*, 352–364. [[CrossRef](#)]
132. Goli, F.; Jamaati, R. Intensifying Goss/Brass texture ratio in AA2024 by asymmetric cold rolling. *Mater. Lett.* **2018**, *219*, 229–232. [[CrossRef](#)]
133. Diniz, S.B.; Benatti, E.A.; Paula, A.S.; Bolmaro, R.E.; Silva, L.C.; Meirelles, B.G. Microstructural evaluation of an asymmetrically rolled and recrystallized 3105 aluminum alloy. *J. Mater. Res. Technol.* **2016**, *5*, 183–189. [[CrossRef](#)]
134. Loorentz; Ko, Y.G. Effect of differential speed rolling strain on microstructure and mechanical properties of nanostructured 5052 Al alloy. *J. Alloy. Compd.* **2014**, *586*, S205–S209. [[CrossRef](#)]
135. Ko, Y.G.; Hamad, K. Microstructure stability and mechanical properties of ultrafine grained 5052 Al alloy fabricated by differential speed rolling. *Mater. Sci. Eng. A* **2018**, *733*, 24–27. [[CrossRef](#)]
136. Tamimi, S.; Correia, J.P.; Lopes, A.B.; Ahzi, S.; Barlat, F.; Gracio, J.J. Asymmetric rolling of thin AA-5182 sheets: Modelling and experiments. *Mater. Sci. Eng. A* **2014**, *603*, 150–159. [[CrossRef](#)]
137. Bintu, A.; Vincze, G.; Picu, R.C.; Lopes, A.B. Effect of symmetric and asymmetric rolling on the mechanical properties of AA5182. *Mater. Des.* **2016**, *100*, 151–156. [[CrossRef](#)]
138. Kraner, J.; Fajfar, P.; Palkowski, H.; Kugler, G.; Godec, M.; Paulin, I. Microstructure and Texture Evolution with Relation to Mechanical Properties of Compared Symmetrically and Asymmetrically Cold Rolled Aluminum Alloy. *Metals* **2020**, *10*, 156. [[CrossRef](#)]
139. Jin, H.; Lloyd, D.J. Effect of a duplex grain size on the tensile ductility of an ultra-fine grained Al-Mg alloy, AA5754, produced by asymmetric rolling and annealing. *Scr. Mater.* **2004**, *50*, 1319–1323. [[CrossRef](#)]
140. Sidor, J.; Petrov, R.H.; Kestens, L.A.I. Deformation, recrystallization and plastic anisotropy of asymmetrically rolled aluminum sheets. *Mater. Sci. Eng. A* **2010**, *528*, 413–424. [[CrossRef](#)]
141. Ko, Y.G.; Chaudry, U.M.; Hamad, K. Microstructure and mechanical properties of AA6061 alloy deformed by differential speed rolling. *Mater. Lett.* **2020**, *259*, 126870. [[CrossRef](#)]
142. Wronski, S.; Bacroix, B. Microstructure evolution and grain refinement in asymmetrically rolled aluminium. *Acta Mater.* **2014**, *76*, 404–412. [[CrossRef](#)]
143. Jin, H.; Lloyd, D.J. Evolution of texture in AA6111 aluminum alloy after asymmetric rolling with various velocity ratios between top and bottom rolls. *Mater. Sci. Eng. A* **2007**, *465*, 267–273. [[CrossRef](#)]
144. Lee, J.-H.; Kim, G.-H.; Nam, S.K.; Kim, I.; Lee, D.N. Calculation of plastic strain ratio of AA1050 Al alloy sheet processed by heavy asymmetric rolling-annealing followed by light rolling-annealing. *Comput. Mater. Sci.* **2015**, *100*, 45–51. [[CrossRef](#)]
145. Dutta, S.; Kaiser, M.S. Effect of asymmetric rolling on formability of pure aluminium. *J. Mech. Eng.* **2015**, *44*, 94–99. [[CrossRef](#)]
146. Zanchetta, B.D.; Da Silva, V.K.; Sordi, V.L.; Rubert, J.B.; Kliauga, A.M. Effect of asymmetric rolling under high friction coefficient on recrystallization texture and plastic anisotropy of AA1050 alloy. *Trans. Nonferrous Met. Soc. China* **2019**, *29*, 2262–2272. [[CrossRef](#)]
147. Shore, D.; Kestens, L.A.I.; Sidor, J.; Houtte, P.V.; Bael, A.V. Process parameter influence on texture heterogeneity in asymmetric rolling of aluminium sheet alloys. *Int. J. Mater. Form.* **2018**, *11*, 297–309. [[CrossRef](#)]
148. Simoes, F.J.P.; Sousa, R.J.A.; Gracio, J.J.A.; Barlat, F.; Yoon, J.W. Mechanical behavior of an asymmetrically rolled and annealed 1050-O sheet. *Int. J. Mech. Sci.* **2008**, *50*, 1372–1380. [[CrossRef](#)]
149. Jiang, J.; Ding, Y.; Zuo, F.; Shan, A. Mechanical properties and microstructures of ultrafine-grained pure aluminum by asymmetric rolling. *Scr. Mater.* **2009**, *60*, 905–908. [[CrossRef](#)]
150. Xu, G.; Cao, X.; Zhang, T.; Duan, Y.; Peng, X.; Deng, Y.; Yin, Z. Achieving high strain rate superplasticity of an Al-Mg-Sc-Zr alloy by a new asymmetrical rolling technology. *Mater. Sci. Eng. A* **2016**, *672*, 98–107. [[CrossRef](#)]
151. Duan, Y.; Xu, G.; Tang, L.; Liu, Y.; Xu, J.; Deng, Y.; Yin, Z. Excellent high strain rate superplasticity of Al-Mg-Sc-Zr alloy sheet produced by an improved asymmetrical rolling process. *J. Alloy. Compd.* **2017**, *715*, 311–321. [[CrossRef](#)]
152. Yang, H.W.; Widiantara, I.P.; Ko, Y.G. Effect of deformation path on texture and tension properties of submicrocrystalline Al-Mg-Si alloy fabricated by differential speed rolling. *Mater. Lett.* **2018**, *213*, 54–57. [[CrossRef](#)]
153. Yu, H.; Lu, C.; Tieu, A.K.; Li, H.J.; Godbole, A.; Zhang, S.H. Special Rolling Techniques for Improvement of Mechanical Properties of Ultrafine-Grained Metal Sheets: A Review. *Adv. Eng. Mater.* **2016**, *18*, 754–769. [[CrossRef](#)]
154. Yu, H.; Tieu, A.K.; Lu, C.; Liu, X.; Liu, M.; Godbole, A.; Kong, C.; Qin, Q. A new insight into ductile fracture of ultrafine-grained Al-Mg alloys. *Sci. Rep.* **2015**, *5*, 9568. [[CrossRef](#)]
155. Shi, J.; Hou, L.; Ma, C.; Zuo, J.; Cui, H.; Zhuang, L.; Zhang, J. Mechanical Properties and Microstructures of 5052 Al Alloy Processed by Asymmetric Cryorolling. *Mater. Sci. Forum* **2016**, *850*, 823–828. [[CrossRef](#)]
156. Magalhaes, D.C.C.; Kliauga, A.M.; Ferrante, M.; Sordi, V.L. Asymmetric cryorolling of AA6061 Al alloy: Strain distribution, texture and age hardening behavior. *Mater. Sci. Eng. A* **2018**, *736*, 53–60. [[CrossRef](#)]
157. Chao, Q.; Cizek, P.; Wang, J.; Hodgson, P.D.; Beladi, H. Enhanced mechanical response of an ultrafine grained Ti-6Al-4V alloy produced through warm symmetric and asymmetric rolling. *Mater. Sci. Eng. A* **2016**, *650*, 404–413. [[CrossRef](#)]
158. Huang, X.; Suzuki, K.; Chino, Y. Improvement of stretch formability of pure titanium sheet by differential speed rolling. *Scr. Mater.* **2010**, *63*, 473–476. [[CrossRef](#)]

159. Li, Z.; Fu, L.; Fu, B.; Shan, A. Effects of annealing on microstructure and mechanical properties of nano-grained titanium produced by combination of asymmetric and symmetric rolling. *Mater. Sci. Eng. A* **2012**, *558*, 309–318. [[CrossRef](#)]
160. Yu, H.; Yan, M.; Li, J.; Godbole, A.; Lu, C.; Tieu, K.; Li, H.; Kong, C. Mechanical properties and microstructure of a Ti-6Al-4V alloy subjected to cold rolling, asymmetric rolling and asymmetric cryorolling. *Mater. Sci. Eng. A* **2018**, *710*, 10–16. [[CrossRef](#)]
161. Wronski, M.; Wierzbanski, K.; Wronski, S.; Bacroix, B.; Lipinski, P. Texture variation in asymmetrically rolled titanium. Study by Finite Element Method with implemented crystalline model. *Int. J. Mech. Sci.* **2014**, *87*, 258–267. [[CrossRef](#)]
162. Stolyarov, V.V.; Zeipper, L.; Mingler, B.; Zehetbauer, M. Influence of post-deformation on CP-Ti processed by equal channel angular pressing. *Mater. Sci. Eng. A* **2008**, *476*, 98–105. [[CrossRef](#)]
163. Zhao, X.; Fu, W.; Yang, X.; Langdon, T.G. Microstructure and properties of pure titanium processed by equal-channel angular pressing at room temperature. *Scr. Mater.* **2008**, *59*, 542–545. [[CrossRef](#)]
164. Terada, D.; Inoue, S.; Tsuji, N. Microstructure and mechanical properties of commercial purity titanium severely deformed by ARB process. *J. Mater. Sci.* **2007**, *42*, 1673–1681. [[CrossRef](#)]